Journal of *Marine Science and Engineering*

MDPI

Article

A Trajectory Tracking Control Method for 6 DoF UUV Based on Event Triggering Mechanism

Yakang Ju [1], Wenyu Cai [1,*], Meiyan Zhang [2,*] and Hao Chen [1]

[1] Zhejiang Province Key Laboratory of Intelligent Vehicle Electronics, Hangzhou Dianzi University, Hangzhou 310018, China
[2] College of Electrical Engineering, Zhejiang University of Water Resources and Electric Power, Hangzhou 310018, China
* Correspondence: caiwy@hdu.edu.cn (W.C.); meiyan19831109@163.com (M.Z.)

Abstract: Trajectory tracking control refers to the movement of an unmanned underwater vehicle (UUV) along a desired trajectory, which is a critical technology for the underwater tasks of UUVs. However, in actual scenarios, the reaction torque of propellers induces roll motion in UUVs, and the communication resource and computational resource of UUVs are limited, which affects the trajectory tracking performance of UUVs severely. Hence, this paper introduces an event triggering mechanism to design the double-loop integrated sliding mode control (EDLISMC), which is used for the trajectory tracking control of UUVs. This method designs the kinematic model and dynamic model of 6 degree of freedom (DoF) UUVs under the influence of reaction torque. Then, this method derives the dual loop integral sliding mode controller and designs the event triggering mechanism based on the relative threshold to reduce unnecessary control signals and improve the control efficiency of UUVs. In addition, this method uses a positive lower bound method to verify that the proposed event triggering mechanism does not have Zeno behavior and adopts the Lyapunov theorem to analyze the stability of EDLISMC. Finally, this paper conducts simulations on the simulink component of MATLAB. The relevant simulation proves that the proposed method can complete the trajectory tracking control of UUVs under the influence of reaction torque and it is superior to other methods in terms of resource consumption.

Keywords: trajectory tracking; UUV; resource consumption; reaction torque; event triggering mechanism; 6 DoF

check for updates

Academic Editor: Lei Wan

Received: 17 March 2025
Revised: 13 April 2025
Accepted: 24 April 2025
Published: 28 April 2025

Citation: Ju, Y.; Cai, W.; Zhang, M.; Chen, H. A Trajectory Tracking Control Method for 6 DoF UUV Based on Event Triggering Mechanism. *J. Mar. Sci. Eng.* **2025**, *13*, 879. https://doi.org/10.3390/jmse13050879

Copyright: © 2025 by the authors. Licensee MDPI, Basel, Switzerland. This article is an open access article distributed under the terms and conditions of the Creative Commons Attribution (CC BY) license (https://creativecommons.org/licenses/by/4.0/).

1. Introduction

As rich marine resources can be used to improve the quality of human life, industry and academia increase their research on marine applications gradually. As an essential tool for exploring marine spaces, unmanned underwater vehicles (UUVs) have emerged. Due to the advantages of portability, intelligence, modularity, and extensive operational range, UUVs are widely used in underwater missions such as military reconnaissance [1], target attacks [2], underwater rescue [3], and pipeline laying [4]. In the process of executing underwater tasks, UUVs address the trajectory tracking control problem, which involves a reasonable and precise controller to perform data collection and detection tasks along a desired trajectory. Hence, the trajectory tracking control of the UUV has become one of the research hotspots. However, this research has the following problems: 1. The dynamic model of the UUV has, for example, fixed multivariate, highly nonlinear, strongly coupled, and uncertain characteristics [5]; 2. UUVs are subject to time-varying external disturbances

during motion, which are difficult to measure or estimate [6]. Therefore, these factors make the trajectory tracking control of the UUV a challenging task.

At present, some scholars propose different trajectory tracking control methods to achieve the trajectory tracking of UUVs. Considering the trajectory tracking problem with limited time, Cui et al. [7] transform the trajectory tracking problem of UUVs through orthogonal decomposition technology and design an adaptive trajectory controller through Hamilton control theorem. Due to the existence of random disturbances in the trajectory tracking control of UUVs, Li et al. [8] design a novel sliding mode control scheme to solve this problem, where the radial basis function neural network is used to estimate external disturbances. In the reference [9], the real-time nonlinear predictive control model is proposed for the trajectory tracking of UUVs. Among them, the barrier function is used to deal with the constraints of trajectory tracking, and the solver is used to solve the control model. Since the chattering problem of trajectory tracking easily affects the control effect, Wan et al. [10] propose a second-order active disturbance rejection controller to solve the chattering problem. Considering the trajectory tracking control of UUVs under environmental disturbances, Ye et al. [11] use the cubic spline algorithm and three-dimensional line-of-sight navigation algorithm to generate tracking trajectories and attitude commands and design a backstepping adaptive sliding mode controller based on nonlinear disturbance observer. Considering that there are too few training samples for trajectory tracking control, Wang et al. [12] use the expert demonstration to obtain good training samples and adopt reinforcement learning to achieve trajectory tracking control for UUVs. In reference [13], the improved super-twisting sliding mode and nonlinear disturbance observer are proposed for the trajectory tracking of UUVs. Among them, the nonlinear disturbance observer is used to estimate external disturbances, and the Sigmoid function is used to improve this controller. Li et al. [14] adopt finite-time terminal sliding mode control as the trajectory tracking controller for UUVs, where the radial basis function neural network is used to estimate disturbance information. Considering the trajectory tracking problem with large curvature, Xu et al. [15] design a trajectory tracking method based on an artificial physical model to ensure the smooth movement of UUV, which creates virtual physical forces between the UUV and the desired trajectory. Li et al. [16] propose an adaptive twisting controller to achieve the trajectory tracking of the UUV, where the sliding mode observer and adaptation are used to reduce the chattering effect of trajectory tracking. According to the dynamic model of 6 degree of freedom (DoF) UUVs, Chen et al. [17] establish the dynamic equation of 4 DoF UUVs affected by mismatched disturbances and design a finite-time disturbance observer for the trajectory tracking of UUVs. Bravo et al. [18] design an adaptive fuzzy controller through fuzzy system theory to improve the robustness of trajectory tracking, which includes a Takagi–Sugeno model and adaptive control laws In reference [19], backstepping control is used to convert tracking errors into control instructions, and an adaptive disturbance observer is designed to reduce the trajectory tracking error of UUVs. Considering that the ocean current interferes with the trajectory tracking of UUVs, Xu et al. [20] design the motion controller of the UUV through model predictive control to enhance tracking accuracy. Considering the composite disturbances in the trajectory tracking of UUVs, Yu et al. [21] propose a trajectory control method based on fuzzy neural network, where the fuzzy radial basis function neural network is used to estimate the composite disturbances. Although the above methods can achieve trajectory tracking control, they face the following challenges:

- In real environments, the UUV usually uses propellers. The rotation of propellers produces reaction torque to affect the roll angle of the UUV, which leads to the roll motion of the UUV. However, the above methods focus on considering the impact of introducing external environmental disturbances to the trajectory tracking of UUVs.

The above methods fail to consider the influence of propellers comprehensively. Therefore, we should design the trajectory tracking control method of UUVs under the influence of reaction torque.

- When performing complex trajectory tracking, the roll angle of UUV impacts trajectory tracking significantly. However, the above methods often use the 5 DoF UUV. In addition, the communication resource and computational resource for UUVs are limited. Hence, the above methods fail to establish the 6 DoF model of UUVs and optimize the resource consumption of UUVs.

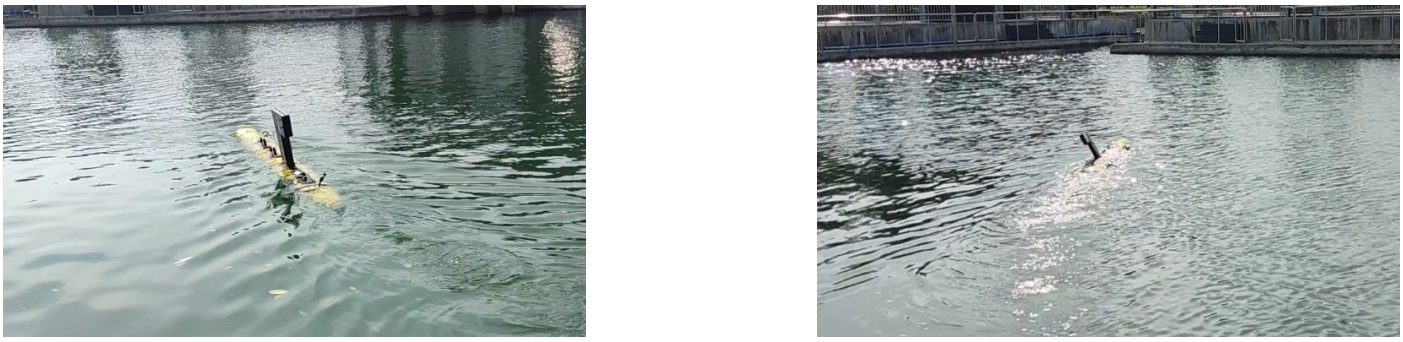
To address the above problems, this paper introduces an event triggering mechanism to design the double-loop integrated sliding mode control (EDLISMC), which is used for the trajectory tracking control method of UUVs. Considering the reaction torque of propellers, this method establishes the kinematic and dynamic models of 6 DoF UUVs. Then, this method derives a dual loop integral sliding mode controller to achieve trajectory tracking control for UUVs, which includes a location loop controller and speed loop controller. In addition, this method designs an event triggering mechanism based on relative threshold to reduce the output frequency of control signals and uses positive lower bound method to prove this mechanism does not have Zeno behavior. Next, this method demonstrates the stability of the proposed controller through the Lyapunov theorem. Hence, the contributions of this paper are described as follows:

- ***Problem***: A scenario for the motion control of 6 DOF UUV under the reaction torque of propeller is established. According to the kinematic model and dynamic model of the UUV, this paper designs the kinematic model and dynamic model of 6-DOF UUVs under the influence of reaction torque, which contributes to the design of corresponding controllers.
- ***Method***: A dual loop integral sliding mode controller is designed to achieve the trajectory tracking control of 6-DOF UUVs. This paper realizes error stabilization through the integral sliding surfaces of position loop controller and speed loop controller. Then, an event triggering mechanism based on relative threshold is proposed to reduce the output frequency of control signals. In addition, the positive lower bound method is used to demonstrate the feasibility of the event triggering mechanism, and the Lyapunov theorem is used to prove the stability of EDLISMC.
- ***Simulation***: The classical scenarios are selected to demonstrate the effectiveness of EDLISMC, which includes a three-dimensional planar cosine trajectory and a three-dimensional spatial spiral trajectory. The relevant simulation proves that EDLISMC can achieve trajectory tracking control under the influence of reaction torque, the maximum triggering interval of the event triggering mechanism is 24 s.

The remainder of this paper is arranged as follows: Section 2 establishes the motion model of the 6 DOF UUV under the reaction torque of propeller. Section 3 discusses the proposed method. Section 4 analyzes the stability of the proposed method. Section 5 analyzes the performance of the proposed method. Section 6 summarizes this paper and future research directions.

2. Problem Description

As we all know, the main propulsion device of the UUV uses propellers, which generate reaction torque. This reaction torque disturbs the roll angle of the UUV, which leads to the tilting phenomenon of UUVs. The straight-line motion and roll motion of the UUV are shown in Figure 1.



(**a**) (**b**)

Figure 1. Impact of counter torque on UUV. (**a**) Initial posture of UUV before straight-line process. (**b**) Posture of UUV after straight-line process.

In addition, the rolling motion of the UUV changes with the variation in propeller thrust. Hence, the thrust F and reaction torque F_Q of UUV can be expressed as:

$$\begin{cases} F = K_T \rho \varpi^2 \\ F_Q = K_Q \rho \varpi^2 \end{cases} \tag{1}$$

where ρ represents the density of seawater. ϖ represents the rotor radius of the propeller, which refers to the distance from the axis of the propeller to the end of the blade. K_T represents the thrust coefficient of the propeller, which is a dimensionless parameter used to measure the thrust intensity that can be generated by the propeller under unit conditions. K_Q represents the reaction torque coefficient of the propeller, which describes the amount of torque required for the propeller to overcome water flow resistance under unit conditions. Furthermore, the connection for F and F_Q is shown as

$$F_Q = \frac{K_Q}{K_T} F \tag{2}$$

Figure 2 is a schematic diagram for the coordinate system of the UUV. In the inertial coordinate system, $\boldsymbol{\eta} = [x, y, z, \phi, \theta, \psi]^T$ is used to represent the location and attitude of the UUV, where x, y, and z are used to represent the surge displacement, sway displacement, and heave displacement of UUV, and ϕ, θ, and ψ are used to represent the roll angle, pitch angle, and yaw of the UUV. In the body-fixed coordinate system, $\boldsymbol{v} = [u, v, w, p, q, r]^T$ is used to represent the linear velocity and angular velocity of the UUV, where u, v, and w are used to represent the surge velocity, sway velocity, and heave velocity of the UUV, and p, q, and r are used to represent the roll velocity, pitch velocity, and yaw velocity of the UUV.

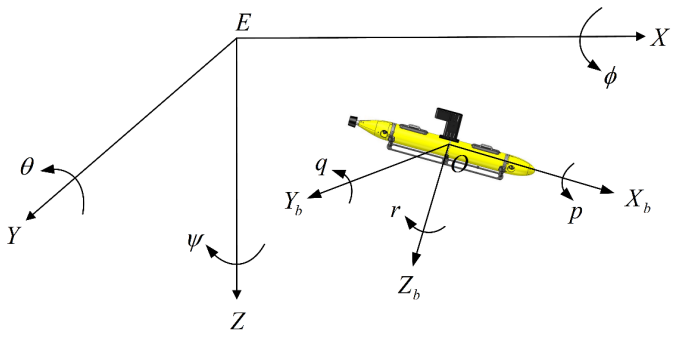


Figure 2. Coordinate system of 6 DoF UUV.

Then, according to the above description, this paper establishes the kinematic model of the 6 DoF UUV, that is,

$$\dot{\boldsymbol{\eta}} = \mathcal{J}(\boldsymbol{\eta})\boldsymbol{v} \tag{3}$$

where $\mathcal{J}(\boldsymbol{\eta})$ is used to represent the Jacobian matrix related to the location and attitude of the UUV. Miao et al. [22,23] analyze the trajectory tracking problem of the UUV and establish the kinematic model of the UUV. Hence, according to the kinematic model of references [22,23], the complete kinematic model of the 6 DoF UUV is established to analyze the influence of the motion speed of the UUV, which can be defined as Equation (4).

$$\begin{cases} \dot{x} = u\cos\psi\cos\theta + v(-\sin\psi\cos\phi + \cos\psi\sin\theta\sin\phi) + w(\sin\psi\sin\phi + \cos\psi\sin\theta\cos\phi) \\ \dot{y} = u\sin\psi\cos\theta + v(\cos\psi\cos\phi + \sin\psi\sin\theta\sin\phi) + w(-\cos\psi\sin\phi + \sin\psi\sin\theta\cos\phi) \\ \dot{z} = -u\sin\theta + v\cos\theta\sin\phi + w\cos\theta\cos\phi \\ \dot{\phi} = p + q\sin\phi\tan\theta + r\cos\phi\tan\theta \\ \dot{\theta} = q\cos\phi - r\sin\phi \\ \dot{\psi} = (q\sin\phi + r\cos\phi)/\cos\theta \end{cases} \tag{4}$$

Similarly, according to the above description, the dynamic model of the 6 DoF UUV is established to discuss the influence of reaction torque.

$$\mathcal{M}\dot{\boldsymbol{v}} + \mathcal{C}(\boldsymbol{v})\boldsymbol{v} + \mathcal{D}(\boldsymbol{v})\boldsymbol{v} + \mathcal{G}(\boldsymbol{\eta}) = \mathcal{T}_v + \mathcal{T}_d + \mathcal{T}_f \tag{5}$$

where $\mathcal{M}$ is used to represent the inertia matrix including added mass. $\mathcal{C}$ is used to represent the Coriolis and centrifugal forces. $\mathcal{D}$ is used to represent the hydrodynamic damping term, and $\mathcal{G}$ is used to represent the restoring force. $\mathcal{T}_v$ is used to represent the control force and moment. $\mathcal{T}_d$ is used to represent the time-varying external disturbance. $\mathcal{T}_f$ is used to represent the reaction torque.

According to the kinematic model of references [22,23] and above equations, the dynamic model of the 6 DoF UUV under the influence of reaction torque is established, which can be expressed as Equation (6).

$$\begin{cases} m_0\dot{u} + m_0[z_G(\dot{q} + rp) + 2(wq - vr)] + (d_{t1}|u| + d_{t2})u = \tau_u + \tau_{ud} \\ m_0\dot{v} + m_0[z_G(-\dot{p} + rq) + 2(ur - wp)] + (d_{t1}|v| + d_{t2})v = \tau_v + \tau_{vd} \\ m_0\dot{u} + m_0[z_G(-p^2 - q^2) + 2(vp - uq)] + (d_{t1}|w| + d_{t2})w = \tau_w + \tau_{wd} \\ I_{xx}\dot{p} + m_0z_G(\dot{v} - ur + pw) + I_rq - I_qr + (d_1|p| + d_2)p + z_Gm_0g\cos\theta\sin\phi = (1 + \frac{K_Q}{K_T})\tau_p + \tau_{pd} \\ I_{yy}\dot{p} + m_0z_G(\dot{u} - rv + qw) + I_rp - I_pr + (d_1|q| + d_2)q + z_Gm_0g\sin\theta = \tau_q + \tau_{qd} \\ I_{zz}\dot{p} + I_qp - I_pq + (d_1|r| + d_2)r = \tau_r + \tau_{rd} \end{cases} \tag{6}$$

Among them, m_0 is the mass; g is the gravitational acceleration; z_G is the longitudinal center height; $I_{xx}, I_{yy}, I_{zz}, I_p, I_q, I_r$ are the moment of inertia coefficients; and d_{t1}, d_{t2}, d_1, d_2 are the damping coefficients.

Due to the limitations existing in external interference, this paper establishes the following conditions to clarify the controller design:

- Condition 1: The estimation error of the system model and the time-varying external disturbances should be constrained. It can be defined as $\max(|\tau_d|) < \tau_{dM}$, where τ_{dM} is an upper limit for external disturbances.
- Condition 2: The system model has an upper limit on reaction torque. It can be defined as $\max(\left|\tau_f\right|) < \tau_{fM}$, where τ_{fM} is an upper limit for reaction torque.
- Condition 3: The system model has an upper limit on thrust. It can be defined as $\max(|\tau|) < \tau_M$, where τ_M is an upper limit for thrust.

- Condition 4: The pitch angle θ of the UUV satisfies $|\theta| < \pi/2$.
- Condition 5: The desired trajectories η_d, $\dot{\eta}_d$, and $\ddot{\eta}_d$ of the UUV are limited.

3. The Proposed Method

3.1. Overall Structure

Integral sliding mode control (ISMC) improves the response speed and anti-interference ability by the sliding mode surface, which is helpful to improve the accuracy of the control process [24,25]. In addition, ISMC is widely used in different fields such as attitude control and formation cooperation [26]. According to the UUV model in Section 2, this paper designs EDLISMC as the trajectory tracking control method for UUVs.

Figure 3 is the major module of EDLISMC to implement the trajectory tracking of the UUV. This method uses dual-loop integral sliding mode control (DLISMC) and an event triggering mechanism. The specific content is summarized as follows:

1. DLISMC includes the location loop controller and the speed loop controller. According to ISMC and the kinematic model of the UUV, the location loop controller realizes the tracking of location and attitude through the expected location and real-time location of the UUV. Then, the location loop controller outputs the reference speed as the input of the speed loop controller. Considering the time-varying ocean disturbances, the speed loop controller analyzes the dynamic model of the UUV under the influence of reaction torque.
2. The proposed event triggering mechanism determines whether to update the thrust output based on the output thrust of the speed loop. The ideal thrust of UUV is generated by EDLISMC. After the thruster is started, the UUV obtains real-time speed feedback to achieve precise tracking of the reference speed.

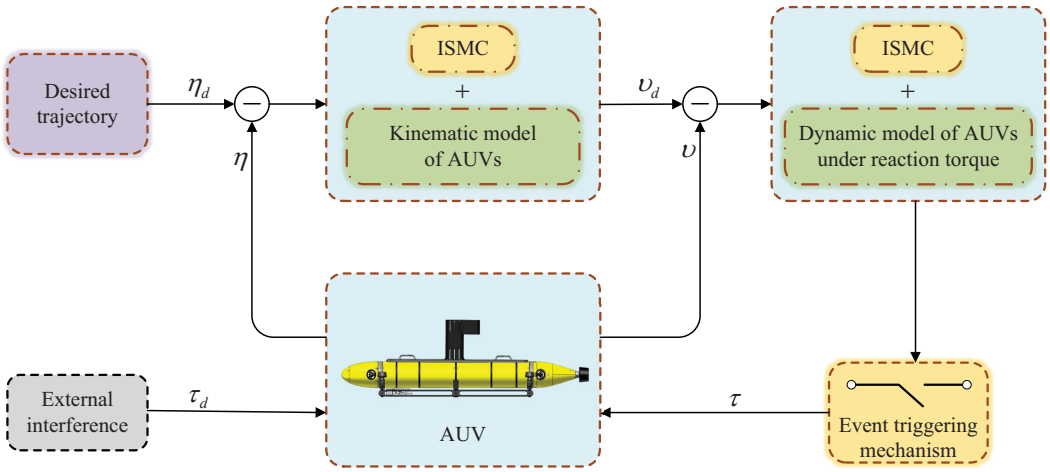


Figure 3. Major modules of EDLISMC.

3.2. Dual-Loop Integral Sliding Mode Control Law

In the location loop controller, this paper defines the location errors x_e, y_e, and z_e and the angle errors ϕ_e, θ_e, and ψ_e through the following equation:

$$\begin{cases} x_e = x - x_d \\ y_e = y - y_d \\ z_e = z - z_d \\ \phi_e = \phi - \phi_d \\ \theta_e = \theta - \theta_d \\ \psi_e = \psi - \psi_d \end{cases} \tag{7}$$

where x_d, y_d, and z_d are used to represent the desired location of the UUV. ϕ_d, θ_d, and ψ_d are used to represent the desired angle of the UUV. x, y, and z are used to represent the actual location of the UUV. ϕ, θ, and ψ are used to represent the actual angle of the UUV. Then, this paper defines the derivatives of the location error and angle error of the UUV through the following equation:

$$\begin{cases} \dot{x}_e = \dot{x} - \dot{x}_d \\ \dot{y}_e = \dot{y} - \dot{y}_d \\ \dot{z}_e = \dot{z} - \dot{z}_d \\ \dot{\phi}_e = \dot{\phi} - \dot{\phi}_d \\ \dot{\theta}_e = \dot{\theta} - \dot{\theta}_d \\ \dot{\psi}_e = \dot{\psi} - \dot{\psi}_d \end{cases} \tag{8}$$

In addition, this paper analyzes the sliding surface of the location control related to x, y, and z and the sliding surface of attitude control related to ϕ, θ, and ψ, which can be described as

$$\begin{cases} S_x = \alpha_1^x x_e + h_x \\ \dot{h}_x = \alpha_2^x x_e, h_x(0) = -\alpha_1^x x_e(0) \end{cases} \tag{9}$$

$$\begin{cases} S_y = \alpha_1^y y_e + h_y \\ \dot{h}_y = \alpha_2^y y_e, h_y(0) = -\alpha_1^y y_e(0) \end{cases} \tag{10}$$

$$\begin{cases} S_z = \alpha_1^z z_e + h_z \\ \dot{h}_z = \alpha_2^z z_e, h_z(0) = -\alpha_1^z z_e(0) \end{cases} \tag{11}$$

$$\begin{cases} S_\phi = h_\phi + \alpha_1^\phi \phi_e \\ \dot{h}_\phi = \alpha_2^\phi \phi_e, h_\phi(0) = -\alpha_1^\phi \phi_e(0) \end{cases} \tag{12}$$

$$\begin{cases} S_\theta = \alpha_1^\theta \theta_e + h_\theta \\ \dot{h}_\theta = \alpha_2^\theta \theta_e, h_\theta(0) = -\alpha_1^\theta \theta_e(0) \end{cases} \tag{13}$$

$$\begin{cases} S_\psi = \alpha_1^\psi \psi_e + h_\psi \\ \dot{h}_\psi = \alpha_2^\psi \psi_e, h_\psi(0) = -\alpha_1^\psi \psi_e(0) \end{cases} \tag{14}$$

where α_1^x, α_2^x, α_1^y, α_2^y, α_1^z, α_2^z, α_1^ϕ, α_2^ϕ, α_1^θ, α_2^θ, α_1^ψ, and α_2^ψ are used to represent the positive constants. The integral sliding surface adopts a constant rate reaching law, which can be described as

$$\dot{S} = -\varepsilon \mathrm{sgn}(S) \tag{15}$$

where ε is used to represent the scalar parameter of the convergence rate. To reduce the chattering caused by sign function $\mathrm{sgn}(\cdot)$, this paper adjusts the sign function to obtain $sat(\cdot)$, which can be described as

$$sat(S) = \begin{cases} S, |S| \leq 0 \\ 1, S > 1 \\ -1, S < -1 \end{cases} \tag{16}$$

According to Equations (9)∼(14), this paper derives the sliding surface of location control S_x, S_y, and S_z and the sliding surface of attitude control S_ϕ, S_θ, and S_ψ. In addition, based on Equations (7), (8), and (15), this paper obtains the following content:

$$\begin{cases} -\varepsilon_x |S_x|^2 sat(S_x) = \alpha_1^x (\dot{x} - \dot{x}_d) + \alpha_2^x x_e \\ -\varepsilon_y |S_y|^2 sat(S_y) = \alpha_1^y (\dot{y} - \dot{y}_d) + \alpha_2^y y_e \\ -\varepsilon_z |S_z|^2 sat(S_z) = \alpha_1^z (\dot{z} - \dot{z}_d) + \alpha_2^z z_e \\ -\varepsilon_\phi |S_\phi|^2 sat(S_\phi) = \alpha_1^\phi (\dot{\phi} - \dot{\phi}_d) + \alpha_2^\phi \phi_e \\ -\varepsilon_\theta |S_\theta|^2 sat(S_\theta) = \alpha_1^\theta (\dot{\theta} - \dot{\theta}_d) + \alpha_2^\theta \theta_e \\ -\varepsilon_\psi |S_\psi|^2 sat(S_\psi) = \alpha_1^\psi (\dot{\psi} - \dot{\psi}_d) + \alpha_2^\psi \psi_e \end{cases} \tag{17}$$

Then, this paper substitutes Equation (4) into Equation (17) to obtain the virtual reference speed u_d, v_d, w_d, p_d, q_d, and r_d, which can be expressed as

$$u_d = \frac{-\alpha_2^x (x - x_d) - \varepsilon_x sat(S_x)}{\alpha_1^x \cos\psi \cos\theta} - \frac{v(-\sin\psi \cos\phi + \cos\psi \sin\theta \sin\phi)}{\cos\psi \cos\theta} - \frac{w(\sin\psi sin\theta + \cos\psi \sin\theta \cos\phi) - \dot{x}_d}{\cos\psi \cos\theta} \tag{18}$$

$$v_d = \frac{-\alpha_2^y (y - y_d) + \varepsilon_y sat(S_y)}{\alpha_1^y (\cos\psi \cos\phi + \sin\psi \sin\theta \sin\phi)} - \frac{u \sin\psi \cos\theta + w(-\cos\psi \sin\phi + \sin\psi \sin\theta \cos\phi) - \dot{y}_d}{(\cos\psi \cos\phi + \sin\psi \sin\theta \sin\phi)} \tag{19}$$

$$w_d = -\frac{\varepsilon_z sat(S_z) + \alpha_2^z (z - z_d)}{\alpha_1^z \cos\theta \cos\phi} - \frac{-u \sin\theta + v \cos\theta \sin\phi - \dot{z}_d}{\cos\theta \cos\phi} \tag{20}$$

$$p_d = \dot{\phi}_d - q \sin\phi \tan\theta + \frac{-\varepsilon_\phi sat(S_\phi) - \alpha_2^\phi (\phi - \phi_d)}{\alpha_1^\phi} - r \cos\phi \tan\theta \tag{21}$$

$$q_d = \frac{-\varepsilon_\theta sat(S_\theta) + \alpha_2^\theta (\phi - \phi_d)}{\alpha_1^\theta \cos\phi} + r \tan\phi + \dot{\theta}_d / \cos\phi \tag{22}$$

$$r_d = -\frac{\varepsilon_\psi sat(S_\psi) + \alpha_2^\psi \psi - \alpha_2^\psi \psi_d}{\alpha_1^\psi \cos\phi} \cos\theta - \frac{\cos\theta}{\cos\phi} \frac{q \sin\phi}{\cos\theta} + \frac{\cos\theta}{\cos\phi} \dot{\psi}_d \tag{23}$$

In the speed loop controller, this paper also defines the virtual linear velocity error u_e, v_e, and w_e and the angular velocity error p_e, q_e, and r_e, which can be expressed as Equation (24).

$$\begin{cases} u_e = u - u_d \\ v_e = v - v_d \\ w_e = w - w_d \\ p_e = p - p_d \\ q_e = q - q_d \\ r_e = r - r_d \end{cases} \tag{24}$$

where u_d, v_d, w_d, p_d, q_d, and r_d are used to represent the virtual reference speed from the location loop controller. u, v, w, p, q, and r are used to represent the actual speed of the UUV. Then, the derivative of virtual reference speed error for the UUV is

$$\begin{cases} \dot{u}_e = \dot{u} - \dot{u}_d \\ \dot{v}_e = \dot{v} - \dot{v}_d \\ \dot{w}_e = \dot{w} - \dot{w}_d \\ \dot{p}_e = \dot{p} - \dot{p}_d \\ \dot{q}_e = \dot{q} - \dot{q}_d \\ \dot{r}_e = \dot{r} - \dot{r}_d \end{cases} \tag{25}$$

In addition, this paper analyzes the sliding surfaces for linear velocity control related to u, v, and w and the sliding mode surfaces for angular velocity control related to p, q, and r, which can be defined as

$$\begin{cases} S_u = \alpha_1^u u_e + h_u \\ \dot{h}_u = \alpha_2^u u_e, h_u(0) = -\alpha_1^u u_e(0) \end{cases} \tag{26}$$

$$\begin{cases} S_v = \alpha_1^v v_e + h_v \\ \dot{h}_v = \alpha_2^v v_e, h_v(0) = -\alpha_1^v v_e(0) \end{cases} \tag{27}$$

$$\begin{cases} S_w = \alpha_1^w w_e + h_w \\ \dot{h}_w = \alpha_2^w w_e, h_w(0) = -\alpha_1^w w_e(0) \end{cases} \tag{28}$$

$$\begin{cases} S_p = \alpha_1^p p_e + h_p \\ \dot{h}_p = \alpha_2^p p_e, h_p(0) = -\alpha_1^p p_e(0) \end{cases} \tag{29}$$

$$\begin{cases} S_q = \alpha_1^q q_e + h_q \\ \dot{h}_q = \alpha_2^q q_e, h_q(0) = -\alpha_1^q q_e(0) \end{cases} \tag{30}$$

$$\begin{cases} S_r = \alpha_1^r r_e + h_r \\ \dot{h}_r = \alpha_2^r r_e, h_r(0) = -\alpha_1^r r_e(0) \end{cases} \tag{31}$$

According to Equations (26)∼(31), this paper derives the sliding surfaces of linear velocity control S_u, S_v, and S_w and the sliding mode surfaces of angular velocity control S_p, S_q, and S_r. In addition, based on Equations (24), (25), and (15), this paper obtains the following content:

$$\begin{cases} -\varepsilon_u |S_u|^2 sat(S_u) = \alpha_1^u (\dot{u} - \dot{u}_d) + \alpha_2^u u_e \\ -\varepsilon_v |S_v|^2 sat(S_v) = \alpha_1^v (\dot{v} - \dot{v}_d) + \alpha_2^v v_e \\ -\varepsilon_w |S_w|^2 sat(S_w) = \alpha_1^w (\dot{w} - \dot{w}_d) + \alpha_2^w w_e \\ -\varepsilon_p |S_p|^2 sat(S_p) = \alpha_1^p (\dot{p} - \dot{p}_d) + \alpha_2^p p_e \\ -\varepsilon_q |S_q|^2 sat(S_q) = \alpha_1^q (\dot{q} - \dot{q}_d) + \alpha_2^q q_e \\ -\varepsilon_r |S_r|^2 sat(S_r) = \alpha_1^r (\dot{r} - \dot{r}_d) + \alpha_2^r r_e \end{cases} \tag{32}$$

Hence, this paper substitutes Equation (6) into Equation (32) to obtain the thrust of UUV τ_u, τ_v, τ_w, τ_p, τ_q, and τ_r, which can be expressed as

$$\begin{aligned} \tau_u = {} & z_G m_0 \dot{q} + z_G m_0 rp + \frac{-m_0 \varepsilon_u sat(S_u)}{\alpha_1^u} + 2m_0 wq - 2m_0 vr \\ & + d_{t_1}|u|u + d_{t_2} u d_{t_1}|u|u + d_{t_2} u + m_0 \dot{u}_d - \frac{m_0 \alpha_2^u}{\alpha_1^u} u + \frac{m_0 \alpha_2^u}{\alpha_1^u} u_d \end{aligned} \tag{33}$$

$$\begin{aligned} \tau_v = {} & -m_0 z_G \dot{p} + m_0 z_G rq - \frac{m_0 \varepsilon_v sat(S_v)}{\alpha_1^v} + 2m_0 (ur - \omega p) \\ & + v d_{t_1}|v| + v d_{t_2} + m_0 \dot{v}_d - \frac{m_0 \alpha_2^v}{\alpha_1^v} v + \frac{m_0 \alpha_2^v}{\alpha_1^v} v_d \end{aligned} \tag{34}$$

$$\begin{aligned} \tau_w = {} & -z_G m_0 p^2 - z_G m_0 q^2 + \frac{-m_0 \varepsilon_w sat(S_w)}{\alpha_1^w} + 2m_0 vp - 2m_0 uq \\ & + d_{t_2} w + d_{t_1}|w|w + m_0 \dot{w}_d + \frac{m_0 \alpha_2^w}{\alpha_1^w} w_d - \frac{m_0 \alpha_2^w}{\alpha_1^w} w \end{aligned} \tag{35}$$

$$\tau_p = m_0 z_G \dot{v} - \frac{I_{xx}\varepsilon_p sat(S_p) + I_{xx}\alpha_2^p(p - p_d)}{\alpha_1^p} - m_0 z_G ur + m_0 z_G pw + z_G m_0 g \cos\theta \sin\phi + d_1|p|p + I_{xx}\dot{p}_d + d_2 p + I_r q - I_q r \quad (36)$$

$$\tau_q = m_0 z_G \dot{u} - \frac{I_{yy}\varepsilon_q sat(S_q) + I_{yy}\alpha_2^q(q - q_d)}{\alpha_1^q} - m_0 z_G rv + m_0 z_G qw + d_1|q|q - I_r p + d_2 q + I_p r + z_G m_0 g \sin\theta + I_{yy}\dot{q}_d \quad (37)$$

$$\tau_r = I_{zz}\dot{r}_d - \frac{I_{zz}\varepsilon_r sat(S_r) + I_{zz}\alpha_2^r(r - r_d)}{\alpha_1^r} + I_q p - I_p q - d_1|r|r - d_2 r \quad (38)$$

3.3. Event Triggering Mechanism

The time triggering controller applies control inputs to the system at a fixed frequency. However, in practical operation, the thrust signal often has significant redundancy, which includes many repeated or slightly varying control inputs that have minimal impact on system performance. The frequent updates of those ineffective control signals fail to improve control performance significantly and lead to the unnecessary consumption of computational and communication resources. To enhance resource utilization efficiency, an event triggering mechanism can be introduced in this method. If the difference between the thrust at the current moment and the thrust at the last trigger moment exceeds a pre-set threshold, the controller updates the thrust output; otherwise, the previous control input is maintained. According to Equations (33)∼(38), the specific event triggering design process is as follows:

The $t_0, t_1, ..., t_k$ represents the time sequence of event triggering, where t_k is the triggering moment. Therefore, the thrust measurement error $e_\tau(t)$ can be defined as

$$e_\tau(t) = \|\tau(t_k) - \tau(t)\| \quad (39)$$

where $t \in [t_k, t_{k+1})$, $k = 1, 2, ..., N$ is used to represent the thrust at the previous moment $t = t_k$. According to the state of the UUV, $\tau(t)$ is used to represent the continuous control signal output by this controller. Considering the triggering strategy of relative thresholds, the event triggering mechanism for the dual-loop integral sliding mode controller can be described as

$$\begin{aligned} &\hat{\tau}(t) = \tau(t_k), t \in [t_k, t_{k+1}] \\ &t_{k+1} = \inf\{t > t_k | f(t, e_\tau(t)) \geq 0\} \end{aligned} \quad (40)$$

where $\hat{\tau}(t)$ is used to represent the final output control signal, and $f(t, e(t))$ is used to represent the event function. If the event function $f(t, e(t)) \geq 0$ within the time interval $t \in [t_k, t_{k+1}]$, the event triggering controller Equation (40) is activated and updated; if this function $f(t, e(t)) < 0$ within the time interval $t \in [t_k, t_{k+1}]$, the event triggering controller retains its value from the previous moment. Then, the event triggering function $f(t, e(t))$ is as follows:

$$f(t, e_\tau(t)) = e_\tau(t) - \sigma|\tau(t)| - \xi \quad (41)$$

where ξ and σ are appropriate positive constants.

3.4. Zeno Behavior Analysis

Zeno behavior refers to the phenomenon where an event triggering mechanism is activated an infinite number of times within a finite period. This scenario is unfeasible in reality and cannot be physically realized. The design of the event triggering mechanism

is a mathematical process. Therefore, it is necessary to analyze whether Zeno behavior exists in the event triggering mechanism. Binh et al. [27] analyze the Zeno behavior of the event triggering mechanism and propose the criteria to eliminate this Zeno behavior. Hence, this paper uses the positive lower bound method to analyze the Zeno behavior of the event triggering mechanism. If there is a positive minimum value for the interval between any two event triggering processes, then this event triggering mechanism does not have Zeno behavior.

This paper derives the thrust measurement error $e_\tau(t)$. Hence, its relevant content can be described as

$$\|\dot{\tau}(t)\| \geq \left\| \frac{d}{dt} e_\tau(t) \right\| = \frac{d}{dt} \|e_\tau(t)\| \tag{42}$$

where $\dot{\tau}(t)$ is the derivative of $\tau(t)$. Since all signals within this system are restricted, we can find a normal constant vector ϖ that satisfies this condition $\|\dot{\tau}(t)\| \leq \varpi$.

According to the initial condition $\tau(t_k) = \tau(t)$ and Equations (39) and (40), this paper contains the following content:

$$\begin{aligned} &\lim_{t \to t_k} |e_\tau(t)| = 0 \\ &\lim_{t \to t_{k+1}} |e_\tau(t)| = \sigma|\tau(t)| + \xi \end{aligned} \tag{43}$$

According to Equations (42) and (43), it is evident that the lower bound of the event triggering interval $\Delta T = t_{k+1} - t_k$ satisfies this condition $\inf(\Delta T)\zeta \geq \min\{|e_\tau(t)|\}$, which can be represented as $\Delta T \geq \frac{\sigma|\tau(t)|+\xi}{\varpi}$. Hence, the minimum triggering interval of the proposed event triggering mechanism is necessarily positive, which proves that this mechanism does not have Zeno behavior.

4. Stability Analysis of Proposed Method

To prove the stability of the design method, this paper conducts a stability analysis for the location loop controller and speed loop controller. The following Lyapunov function is selected in this paper for the speed loop controller:

$$V_1 = \frac{1}{2}S_u^2 + \frac{1}{2}S_v^2 + \frac{1}{2}S_w^2 + \frac{1}{2}S_p^2 + \frac{1}{2}S_q^2 + \frac{1}{2}S_r^2 \tag{44}$$

Then, this paper differentiates V_1 and substitutes Equations (26)∼(31) into Equation (44) to obtain Equation (45).

$$\begin{aligned} \dot{V}_1 &= \dot{S}_u S_u + \dot{S}_v S_v + \dot{S}_w S_w + \dot{S}_p S_p + \dot{S}_q S_q + \dot{S}_r S_r \\ &= S_u[\alpha_1^u(\dot{u} - \dot{u}_d) + \alpha_2^u(u - u_d)] + S_v[\alpha_1^v(\dot{v} - \dot{v}_d) + \alpha_2^v(v - v_d)] \\ &+ S_w[\alpha_1^w(\dot{w} - \dot{w}_d) + \alpha_2^w(w - w_d)] + S_p[\alpha_1^p(\dot{p} - \dot{p}_d) + \alpha_2^p(p - p_d)] \\ &+ S_q[\alpha_1^q(\dot{q} - \dot{q}_d) + \alpha_2^q(q - q_d)] + S_r[\alpha_1^r(\dot{r} - \dot{r}_d) + \alpha_2^r(r - r_d)] \end{aligned} \tag{45}$$

According to equations Equation (39) to Equation (41), it can be seen that there exist functions $\lambda_1(t)$ and $\lambda_2(t)$ that satisfy $|\lambda_1(t)|, |\lambda_2(t)| \leq 1$, such that the following holds:

$$\hat{\tau}(t) = [1 + \sigma\lambda_1(t)]\tau(t) + \lambda_2(t)\xi \tag{46}$$

Then, this paper substitutes Equations (6) and (46) into Equation (45) to obtain the following equation:

$$\begin{aligned}\dot{V}_1 = {} & S_u\{\alpha_2^u u + \alpha_1^u[2vr + \frac{\hat{\tau}_u + \tau_{ud} - ud_{t1}|u| - ud_{t2}}{m_0} - z_G rp - \dot{u}_d - 2wq - z_G\dot{q}] - \alpha_2^u u_d\} \\ & + S_v\{\alpha_2^v v + \alpha_1^v[z_G\dot{p} + \frac{\hat{\tau}_v + \tau_{vd} - vd_{t1}|v| - vd_{t2}}{m_0} - z_G rq - 2ur + 2wp - \dot{v}_d] - \alpha_2^v v_d\} \\ & + S_w\{\alpha_2^w w + \alpha_1^w[z_G q^2 + \frac{\hat{\tau}_w + \tau_{wd} - wd_{t1}|w| - wd_{t2}}{m_0} + z_G p^2 - 2vp + 2uq - \dot{w}_d] + \alpha_2^w w_d\} \\ & + S_p\{\alpha_2^p p - \alpha_2^p p_d + \alpha_1^p[\frac{(1+\frac{K_Q}{K_T})\hat{\tau}_p + \tau_{p_d} - m_0 z_G\dot{v} + m_0 z_G ur - m_0 z_G pw)}{I_{xx}} \\ & - \frac{-I_r q + I_q r - d_1|p|p - d_2 p - z_G m_0 g\cos\theta\sin\phi}{I_{xx}} - \dot{P}_d]\} \\ & + S_q\{\alpha_2^q q - \alpha_2^q q_d + \alpha_1^q[\frac{\hat{\tau}_q + \tau_{q_d} - m_0 z_G\dot{u} + m_0 z_G rv - m_0 z_G qw}{I_{yy}} \\ & - \frac{-I_r p + I_p r - d_1|q|q - d_2 q - z_G m_0 g\sin\theta}{I_{y_y}} - \dot{q}_d]\} \\ & + S_r\{\alpha_2^r r - \alpha_2^r r_d + \alpha_1^r[\frac{\hat{\tau}_r + \tau_{rd} - I_q p + I_p q - rd_1|r| - rd_2}{I_{zz}} - \dot{r}_d]\} \end{aligned} \tag{47}$$

Next, this paper substitutes Equations (33)∼(38) into Equation (47) to obtain the following content:

$$\begin{aligned}\dot{V}_1 = {} & S_u\{\alpha_1^u[\frac{-\varepsilon_u sat(S_u) - \alpha_2^u(u-u_d)}{\alpha_1^u} + \frac{\lambda_1(t)\sigma\tau_u + \lambda_2(t)\xi + \tau_{ud}}{m_0}] + \alpha_2^u(u-u_d)\} \\ & + S_v\{\alpha_1^v[\frac{-\varepsilon_v sat(S_v) - \alpha_2^v(v-v_d)}{\alpha_1^v} + \frac{\lambda_1(t)\sigma\tau_v + \lambda_2(t)\xi + \tau_{vd}}{m_0}] + \alpha_2^v(v-v_d)\} \\ & + S_w\{\alpha_1^w[\frac{-\varepsilon_w sat(S_w) - \alpha_2^w(w-w_d)}{\alpha_1^w} + \frac{\lambda_1(t)\sigma\tau_w + \lambda_2(t)\xi + \tau_{wd}}{m_0}] + \alpha_2^w(w-w_d)\} \\ & + S_p\{\alpha_1^p[\frac{(\frac{K_Q}{K_T} + \lambda_1(t)\sigma)\tau_p + \lambda_2(t)\xi + \tau_{p_d}}{I_{xx}} - \frac{\varepsilon_p \mathrm{sat}(S_p) + \alpha_2^p(p-p_d)}{\alpha_1^p}] + \alpha_2^p(p-p_d)\} \\ & + S_q\{\alpha_1^q[\frac{\lambda_1(t)\sigma\tau_q + \lambda_2(t)\xi + \tau_{q_d}}{I_{yy}} - \frac{\varepsilon_q \mathrm{sat}(S_q) + \alpha_2^q(q-q_d)}{\alpha_1^q}] + \alpha_2^q(q-q_d)\} \\ & + S_r\{\alpha_1^r[\frac{\lambda_1(t)\sigma\tau_r + \lambda_2(t)\xi + \tau_{rd}}{I_{zz}} - \frac{\varepsilon_r \mathrm{sat}(S_r) + \alpha_2^r(r-r_d)}{\alpha_1^r}] + \alpha_2^r(r-r_d)\} \end{aligned} \tag{48}$$

According to Condition 1, Condition 2, Condition 3, and Equation (48), this paper obtains Equation (49).

$$\begin{aligned}\dot{V}_1 \le {} & -\varepsilon_u|S_u| - \varepsilon_v|S_v| - \varepsilon_w|S_w| + [\lambda_1(t)\sigma\tau_M + \lambda_2(t)\xi + \tau_{dM}]\frac{S_u\alpha_1^u + S_v\alpha_1^v + S_w\alpha_1^w}{m_0} \\ & -\varepsilon_p|S_p| - \varepsilon_q|S_q| - \varepsilon_w|S_w| + \frac{S_p\alpha_1^p[\lambda_1(t)\sigma\tau_M + \lambda_2(t)\xi + \tau_{dM} + \tau_{fM}]}{I_{xx}} \\ & + \frac{S_q\alpha_1^q[\lambda_1(t)\sigma\tau_M + \lambda_2(t)\xi + \tau_{dM}]}{I_{yy}} + \frac{S_r\alpha_1^r[\lambda_1(t)\sigma\tau_M + \lambda_2(t)\xi + \tau_{dM}]}{I_{zz}} \\ & \le |S_u|[\frac{\alpha_1^u(\sigma\tau_M + \xi + \tau_{dM})}{m_0} - \varepsilon_u] + |S_v|[\frac{\alpha_1^v(\sigma\tau_M + \xi + \tau_{dM})}{m_0} - \varepsilon_v] \\ & + |S_w|[\frac{\alpha_1^w(\sigma\tau_M + \xi + \tau_{dM})}{m_0} - \varepsilon_w] + |S_p|[\frac{\alpha_1^p(\sigma\tau_M + \xi + \tau_{dM} + \tau_{fM})}{I_{xx}} - \varepsilon_p] \\ & + |S_q|[\frac{\alpha_1^q(\sigma\tau_M + \xi + \tau_{dM})}{I_{yy}} - \varepsilon_q] + |S_r|[\frac{\alpha_1^r(\sigma\tau_M + \xi + \tau_{dM})}{I_{zz}} - \varepsilon_r] \end{aligned} \tag{49}$$

According to the Lyapunov theorem, the sliding surfaces of Equation (26) to Equation (31) converge to zero only if the following conditions are satisfied:

$$\begin{cases} \varepsilon_u > {m_0}^{-1}\alpha_1^u(\sigma T_M + \xi + T_{dM}) \\ \varepsilon_v > {m_0}^{-1}\alpha_1^v(\sigma T_M + \xi + T_{dM}) \\ \varepsilon_w > {m_0}^{-1}\alpha_1^w(\sigma T_M + \xi + T_{dM}) \\ \varepsilon_p > {I_{xx}}^{-1}\alpha_1^p(\sigma T_M + \xi + T_{dM} + T_{fM}) \\ \varepsilon_q > {I_{yy}}^{-1}\alpha_1^q(\sigma T_M + \xi + T_{dM}) \\ \varepsilon_r > {I_{zz}}^{-1}\alpha_1^r(\sigma T_M + \xi + T_{dM}) \end{cases} \tag{50}$$

where I_{xx}, I_{yy}, and I_{zz} are the non-zero moment of inertia of the 6-DoF UUV, and m_0 is the non-zero mass. α_1^u, α_1^v, α_1^w, α_1^p, α_1^q, and α_1^r are non-zero constants. ε_u, ε_v, ε_w, ε_p, ε_q, and ε_r are bounded normal constants. Therefore, the above demonstrates that the proposed speed loop controller can remain stable.

The following Lyapunov function is selected in this paper for the location loop controller:

$$V_2 = \frac{1}{2}(S_x^2 + S_y^2 + S_z^2 + S_\phi^2 + S_\theta^2 + S_\psi^2) \tag{51}$$

Then, this paper differentiates V_2 and substitutes Equations (9)∼(14) into Equation (51) to obtain Equation (52). This paper substitutes Equation (6) into Equation (52) to obtain Equation (53).

$$\begin{aligned} \dot{V}_2 &= \dot{S}_x S_x + \dot{S}_y S_y + \dot{S}_z S_z + \dot{S}_\phi S_\phi + \dot{S}_\theta S_\theta + \dot{S}_\psi S_\psi \\ &= S_x[\alpha_1^x \dot{x} + \alpha_2^x x - \alpha_1^x \dot{x}_d - \alpha_2^x x_d] + S_y[\alpha_1^y \dot{y} + \alpha_2^y y - \alpha_1^y \dot{y}_d - \alpha_2^y y_d] \\ &+ S_z[\alpha_1^z \dot{z} + \alpha_2^z z - \alpha_1^z \dot{z}_d - \alpha_2^z z_d] + S_\phi[\alpha_1^\phi \dot{\phi} + \alpha_2^\phi \phi - \alpha_1^\phi \dot{\phi}_d - \alpha_2^\phi \phi_d] \\ &+ S_\theta[\alpha_1^\theta \dot{\theta} + \alpha_2^\theta \theta - \alpha_1^\theta \dot{\theta}_d - \alpha_2^\theta \theta_d] + S_\psi[\alpha_1^\psi \dot{\psi} + \alpha_2^\psi \psi - \alpha_1^\psi \dot{\psi}_d - \alpha_2^\psi \psi_d] \end{aligned} \tag{52}$$

$$\begin{aligned} \dot{V}_2 &= S_x\{\alpha_2^x x + \alpha_1^x[-v\cos\phi\sin\psi + u\cos\theta\cos\psi + v\cos\psi\sin\phi\sin\theta) \\ &+ w\sin\phi\sin\psi + w\sin\theta\cos\psi\cos\phi - \dot{x}_d] - \alpha_2^x x_d\} \\ &+ S_y\{\alpha_2^y y + \alpha_1^y[v\cos\phi\cos\psi + u\cos\theta\sin\psi + v\sin\theta\sin\psi\sin\phi \\ &- w\cos\psi\sin\phi + w\sin\psi\cos\phi\sin\theta - \dot{y}_d] - \alpha_2^y y_d)\} \\ &+ S_z\{\alpha_2^z z + \alpha_1^z[v\sin\phi\cos\theta - u\sin\theta - \dot{z}_d + w\cos\theta\cos\phi] - \alpha_2^z z_d\} \\ &+ S_\phi\{\alpha_2^\theta \theta + \alpha_1^\phi[p + q\tan\theta\sin\phi - \dot{\phi}_d + r\tan\theta\cos\phi] \\ &+ \alpha_2^\phi(\phi - \phi_d)\} + S_\theta\{\alpha_1^\theta[q\cos\phi - r\sin\phi - \dot{\theta}_d] - \alpha_2^\theta\theta_d)\} \\ &+ S_\psi\{\alpha_2^\psi \psi + \alpha_1^\psi[(q\sin\phi + r\cos\phi)/\cos\theta - \dot{\psi}_d] - \alpha_2^\psi\psi_d)\} \end{aligned} \tag{53}$$

Next, this paper substitutes Equations (18)∼(23) into Equation (53) to obtain the following content:

$$
\begin{aligned}
\dot{V}_2 = {} & S_x\{\alpha_1^x[\frac{-\alpha_2^x(x-x_d)-\varepsilon_x sat(S_x)}{\alpha_1^x}]+\alpha_2^x(x-x_d)\} \\
& + S_y\{\alpha_1^y[\frac{-\alpha_2^y(y-y_d)-\varepsilon_y sat(S_y)}{\alpha_1^y}]+\alpha_2^y(y-y_d)\} \\
& + S_z\{\alpha_1^z[\frac{-\alpha_2^z(z-z_d)-\varepsilon_z sat(S_z)}{\alpha_1^z}]+\alpha_2^z(z-z_d)\} \\
& + S_\phi\{\alpha_1^\phi[\frac{-\alpha_2^\phi(\phi-\phi_d)-\varepsilon_\phi sat(S_\phi)}{\alpha_1^\phi}]+\alpha_2^\phi(\phi-\phi_d)\} \\
& + S_\theta\{\alpha_1^\theta[\frac{-\alpha_2^\theta(\theta-\theta_d)-\varepsilon_\theta sat(S_\theta)}{\alpha_1^\theta}]+\alpha_2^\theta(\theta-\theta_d)\} \\
& + S_\psi\{\alpha_1^\psi[\frac{-\alpha_2^\psi(\psi-\psi_d)-\varepsilon_\psi sat(S_\psi)}{\alpha_1^\psi}]+\alpha_2^\psi(\psi-\psi_d)\} \\
\leq {} & -S_x\varepsilon_x sat(S_x) - S_y\varepsilon_y sat(S_y) - S_z\varepsilon_z sat(S_z) \\
& - S_\phi\varepsilon_\phi sat(S_\phi) - S_\theta\varepsilon_\theta sat(S_\theta) - S_\psi\varepsilon_\psi sat(S_\psi) \\
\leq {} & -\varepsilon_x|S_x| - \varepsilon_y|S_y| - \varepsilon_z|S_z| - \varepsilon_\phi|S_\phi| - \varepsilon_\theta|S_\theta| - \varepsilon_\psi|S_\psi|
\end{aligned} \tag{54}
$$

It can be seen from Equation (54) that $\dot{V}_2 \leq 0$. Hence, the designed virtual reference speed in Equation (18) to Equation (23) can ensure the stability of the location loop controller. It can be seen from Equations (49) and (54) that the location loop controller and location loop controller can achieve a stable state, which demonstrates the stability of the entire system.

5. Simulation and Analysis

5.1. Simulation Setup

As shown in Figure 4, this paper uses the Simulink component of MATLAB 2011b to carry out simulations in different scenarios. In addition, this simulation experiment has the following characteristics:

- To demonstrate the performance advantages of EDLISMC, this simulation experiment compares it with proportional integral derivative (PID) [28], dual-layer proportional integral derivative (DLPID) [29], and DLISMC. The location error and angle error of the UUV are the inputs of PID, and then the thrust magnitude of the UUV is obtained through proportional operation, integral operation, and differential operation of PID. DLPID is composed of a location loop controller and a speed loop controller, where the controllers are controlled by PID.
- Table 1 presents the parameter of the UUV mathematical model under reaction torque. The maximum thrust of UUV is set to ± 200 N, and the time-triggered interval is 0.1 s. In addition, the simulation experiment of this paper introduces time-varying external disturbances with different amplitudes and periods, whose values can be expressed as

$$
\begin{cases}
\tau_{ud} = -10 \times \sin(0.6t) \\
\tau_{vd} = -9 \times \sin(0.5t) \\
\tau_{wd} = -3 \times \sin(0.4t) \\
\tau_{p_d} = -4 \times \sin(0.45t) \\
\tau_{q_d} = -2 \times \sin(0.3t) \\
\tau_{rd} = -6 \times \sin(0.1t)
\end{cases} \tag{55}
$$

- To verify the feasibility of EDLISMC, this simulation experiment sets two trajectory tracking scenarios, which include three-dimensional planar cosine trajectory and three-dimensional spatial spiral trajectory. $x(0) = 10$ m, $y(0) = 5$ m, $z(0) = 10$ m,

$\phi(0) = 0.1$ rad, $\theta(0) = 0$ rad, $\psi(0) = 0.1$ rad, $u(0) = v(0) = w(0) = 0$ m/s, and $p(0) = q(0) = r(0) = 0$ rad/s are set as the initial state of the UUV. In terms of parameter selection, this simulation experiment adopts the method of controlling variables to discuss the influence of parameters. After multiple parameter adjustments, this simulation experiment selects the appropriate control parameters. We obtain the main parameters of EDLISMC through extensive testing and the parameter selection of reference [30,31], which are summarized in Table 2.

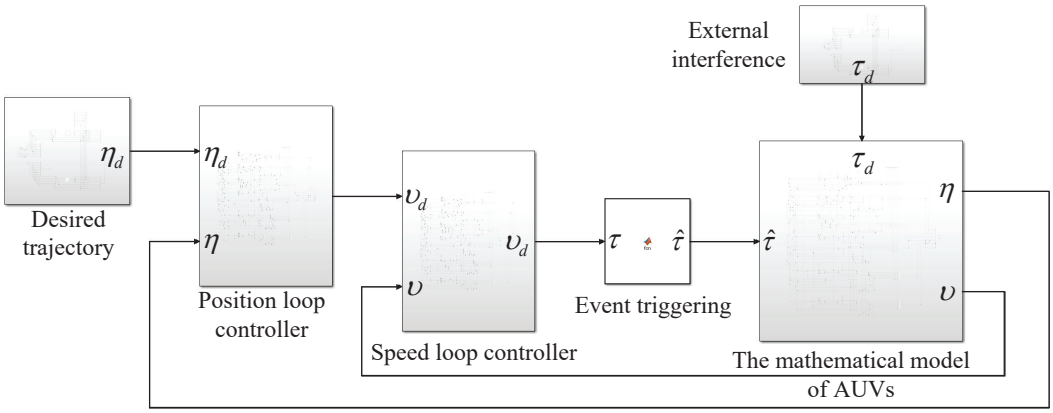


Figure 4. Major modules of EDLISMC.

Table 1. Parameters of UUV mathematical model.

Parameter	Value	Unit	Parameter	Value	Unit
m_0	125	k	K_Q	0.027	/
z_G	0.05	m	K_T	0.063	/
g	9.81	m/s^2	d_2	230	$N{\cdot}s^2/m$
I_{xx}	4.63	$kg{\cdot}m^2$	d_1	280	$N{\cdot}s^2/m$
I_{yy}	4.63	$kg{\cdot}m^2$	d_{t2}	100	$N(s/m)^2v$
I_{zz}	4.63	$kg{\cdot}m^2$	d_{t1}	148	$N(s/m)^2$
I_p	4.63	$kg{\cdot}m^2$	I_r	4.63	$kg{\cdot}m^2$
I_q	4.63	$kg{\cdot}m^2$			

Table 2. Parameters of EDLISMC controller.

Parameter	Value	Parameter	Value	Parameter	Value
α_1^x	0.00001	α_2^x	100,000	ξ	10
α_1^y	0.00001	α_2^y	100,000	σ	0.01
α_1^z	0.0001	α_2^z	900,000	α_2^r	1.2
α_1^ϕ	0.01	α_2^ϕ	5	α_1^r	0.001
α_1^θ	0.01	α_2^θ	0.5	α_2^q	1
α_1^ψ	10	α_2^ψ	5	α_1^q	1
α_1^u	0.001	α_2^u	100	α_2^p	0.5
α_1^v	0.001	α_2^v	0.1	α_1^p	0.01
α_1^w	0.001	α_2^w	0.1		

Due to the limited length of this paper, we provide a brief description of the parameter selection of this paper. In the dual loop integral sliding mode control, parameters α_1^x, α_1^y, α_1^z, α_1^ϕ, α_1^θ, α_1^ψ, α_2^x, α_2^y, α_2^z, α_2^ϕ, α_2^θ, and α_2^ψ act on the proportional term (current error weight) and integral term (cumulative error weight) in the outer loop sliding mode surface, respectively. If the α_1^x, α_1^y, α_1^z, α_1^ϕ, α_1^θ, and α_1^ψ increase, the sensitivity instantaneous position error of the system is enhanced, which easily generates the overshoot and jitter of the system; If the α_1^x, α_1^y, α_1^z, α_1^ϕ, α_1^θ, and α_1^ψ decrease, the response speed, overshoot, and steady-state accuracy

of the system decrease. The reason is that the larger the proportional term coefficient, the steeper the slope of sliding surface, and the faster the system reaches the sliding surface. If the α_2^y, α_2^z, α_2^ϕ, α_2^θ, and α_2^ψ increase, the punishment of the accumulated errors increases and the steady-state deviation of the system decreases. If the α_2^y, α_2^z, α_2^ϕ, α_2^θ, and α_2^ψ decrease, the response speed of the system decreases and the steady-state error of the system increases. The essence of the integral term is to correct system deviations continuously, which can ensure the steady-state performance of the system in the low-frequency range.

In the inner loop sliding surface, the parameters α_1^u, α_1^v, α_1^w, α_1^p, α_1^q, and α_1^r adjust the weight of the proportional term, which has a significant impact on the transient response of the velocity error. If the α_1^u, α_1^v, α_1^w, α_1^p, α_1^q, and α_1^r increase, the response speed of the inner loop increases and the speed loop regulation capability is enhanced, which cause the overshoot and jitter of the inner loop; If the α_1^u, α_1^v, α_1^w, α_1^p, α_1^q, and α_1^r decrease, the response speed of the inner loop reduces, which makes the system become sluggish. The reason is that the slope of the sliding surface can control the convergence rate of error towards the sliding surface. Then, the parameters α_2^u, α_2^v, α_2^w, α_2^p, α_2^q, and α_2^r are the integral coefficients of the inner loop. If the α_2^u, α_2^v, α_2^w, α_2^p, α_2^q, and α_2^r increase, the steady-state velocity error of the inner loop decreases, and the overshoot of the system is improved; If the α_2^u, α_2^v, α_2^w, α_2^p, α_2^q, and α_2^r decrease, the system response becomes smoother and the steady-state error of the system increases.

The $\sigma \in (0, 1)$ of the event triggering mechanism is the relative threshold coefficient, which measures the triggering sensitivity of error relative to the signal amplitude. $\xi > 0$ is a fixed threshold parameter that provides the lowest triggering threshold when the signal is small, which can avoid the frequent triggering of the event triggering mechanism by noise or quantization jitter. If the σ increases, the triggering frequency of the control signal decreases, which decreases the response speed of the system; If the σ decreases, the triggering frequency of the control signal increases, which increases the resource consumption of the system. If the ξ increases, the triggering frequency of the control signal decreases in the steady-state stage, which increases the steady-state error of the system; If the ξ decreases, the triggering of the control signal is sensitive in the steady-state stage, which leads to an increase in the jitter triggering of the system.

5.2. Simulation Results

5.2.1. Results of Scenario 1

In Scenario 1, the UUV verifies the tracking performance of the EDLISMC controller through three-dimensional planar cosine trajectory tracking, where the experimental duration is 100 s. In the geodetic coordinate framework, the ideal planar cosine trajectory can be described by the following equation:

$$\begin{cases} x_d(t) = 10 \times \sin(0.025\pi t) \\ y_d(t) = 10 \times \cos(0.025\pi t) \\ z_d(t) = 1 + 0.25 \times t \\ \psi_d(t) = 0.025 \times \pi t \\ \theta_d(t) = -\arctan(1/\pi) \\ \phi_d(t) = 0 \end{cases} \tag{56}$$

Figure 5 shows a three-dimensional spatial graph of UUV trajectory tracking under different control methods in Scenario 1. In Figure 5, the red five-pointed star is used to represent the starting location of the UUV, where the initial point is set at an arbitrary position outside the trajectory. The blue five-pointed star is used to represent the end point of the UUV, where the UUV finally arrives. After the experiment starts, the UUV starts to move according to different control algorithms. The final four control methods can make

the UUV track the ideal trajectory. It is obvious that DLISMC and EDLISMC are faster than PID and DLPID.

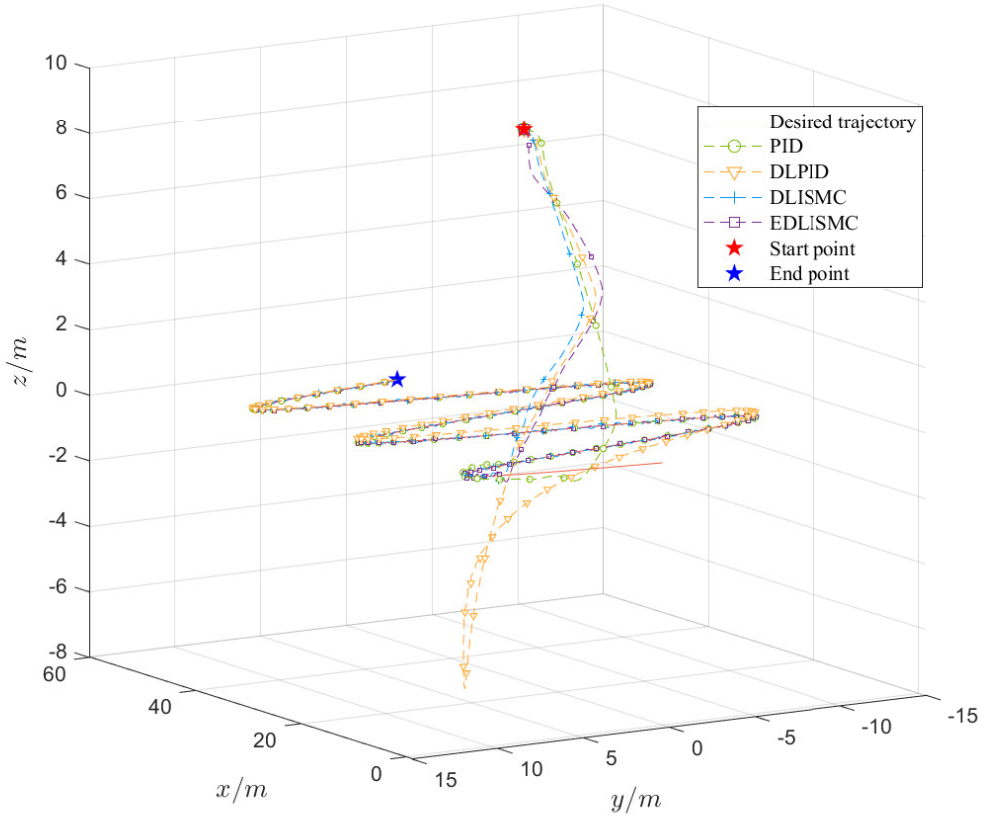


Figure 5. Trajectory tracking of different control methods in Scenario 1.

Figure 6 is the location tracking error of the UUV in Scenario 1. It can be seen from Figure 6 that the four methods can make the location tracking error reach the convergence state, where the location tracking errors of all control methods converge to 0.05 m. Among them, in terms of the convergence speed in the X direction and Y direction, PID is relatively slow, and the other three algorithms are not much different. In terms of the convergence speed in the Z direction, DLPID is relatively slow. The results of Figure 6 also verify the strong robustness and fast convergence characteristics of ISMC. Figure 7 is the angular tracking error of the UUV in Scenario 1, where the angular tracking errors of all control methods converge to 0.005 rad. It can be seen from the figure that there is an obvious chattering phenomenon in the initial stage of EDLISMC. This is because the angle error is relatively large in the initial stage of tracking, which leads to the sharp change in the thrust output of the UUV. As the system stabilizes after running for a period of time, the angular tracking error of EDLISMC converges gradually.

Figure 8 is the linear velocity tracking error of the UUV in Scenario 1, where the linear velocity tracking errors of all control methods converge to 0.2 m/s. It can be seen from Figure 8 that the stability of PID on u and v is worse than that of other control methods, which verifies the advantages of the double-loop framework. Figure 9 shows the angular velocity tracking error of different control methods in Scenario 1, where the angular velocity tracking errors of all control methods converge to 0.02 rad/s. Although all control methods achieve the effective suppression of angular velocity error, these methods have significant differences in response speed and dynamic performance. PID suffers from slow response and insufficient steady-state accuracy. DLPID improves response speed through disturbance feedforward. DLISMC enhances system robustness and convergence through sliding mode control. EDLISMC based on the event triggering mechanism deals

with chattering effectively in the initial stage, which has the best overall performance. It can be seen from Figures 8 and 9 that there is a slight chattering in both DLISMC and EDLISMC. The reason for this phenomenon is: 1. The design of the sliding mode surface and the approaching rate make it difficult to avoid slight chattering. 2. In the initial stage of trajectory tracking, event triggering is frequent.

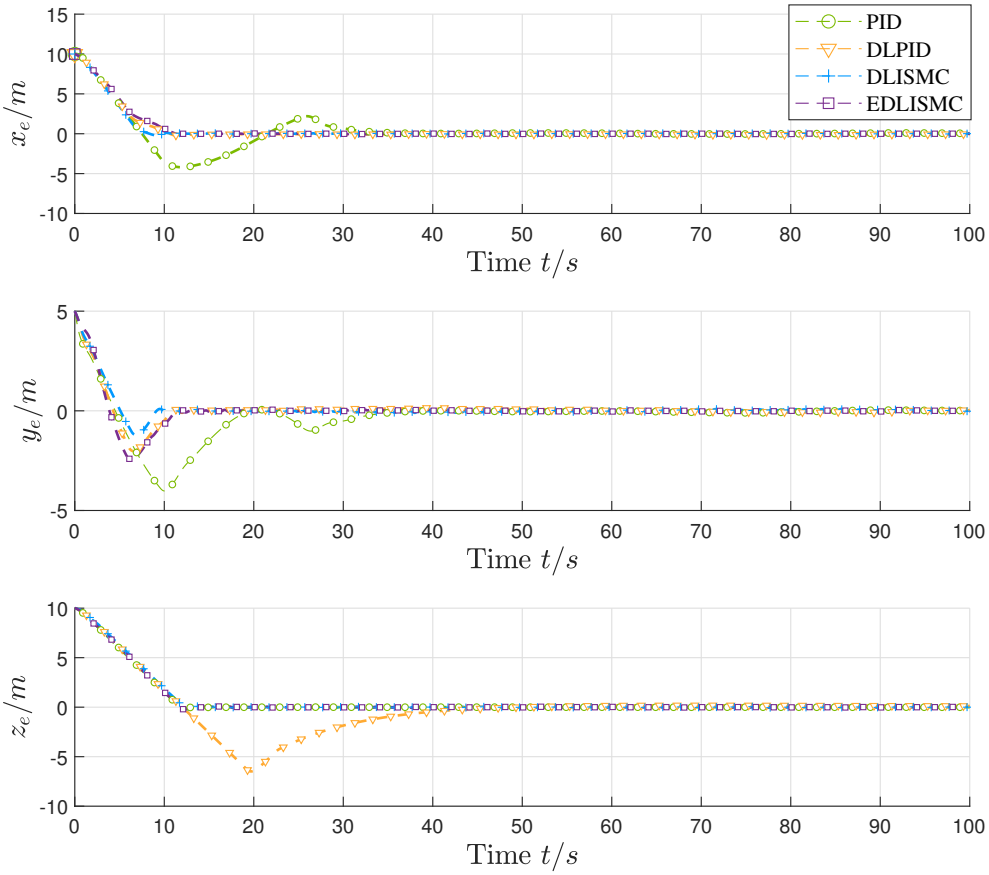


Figure 6. Location tracking error of different control methods in Scenario 1.

Figure 10 shows the trigger accumulation of different thrusts under the time triggering mechanism and event triggering mechanism in Scenario 1, where the horizontal coordinate is time and the vertical coordinate is the number of triggers. Table 3 provides the specific values of trigger accumulation. Since the time triggering mechanism adopts a fixed sampling period (0.1 s in this experiment), the controller performs a total of 1000 control updates within the 100 s experimental duration, which makes a deterministic number of updates. In contrast, the event triggering mechanism determines the update instants dynamically based on variations in the control input. The number of control updates thus reflects the frequency of significant changes in the thrust signal, which can be regarded as the actual count of thrust update events. It can be seen from Figure 10 and Table 3 that compared with time triggering, the event triggering mechanism reduces the output frequency of control signals significantly, and the decrease range of the control signal τ_r is relatively limited. The reason for this phenomenon is that there are fewer redundant signals in the yaw angle control. In conclusion, the proposed event triggering mechanism avoids the output of a large number of redundant control signals effectively and reduces resource consumption significantly.

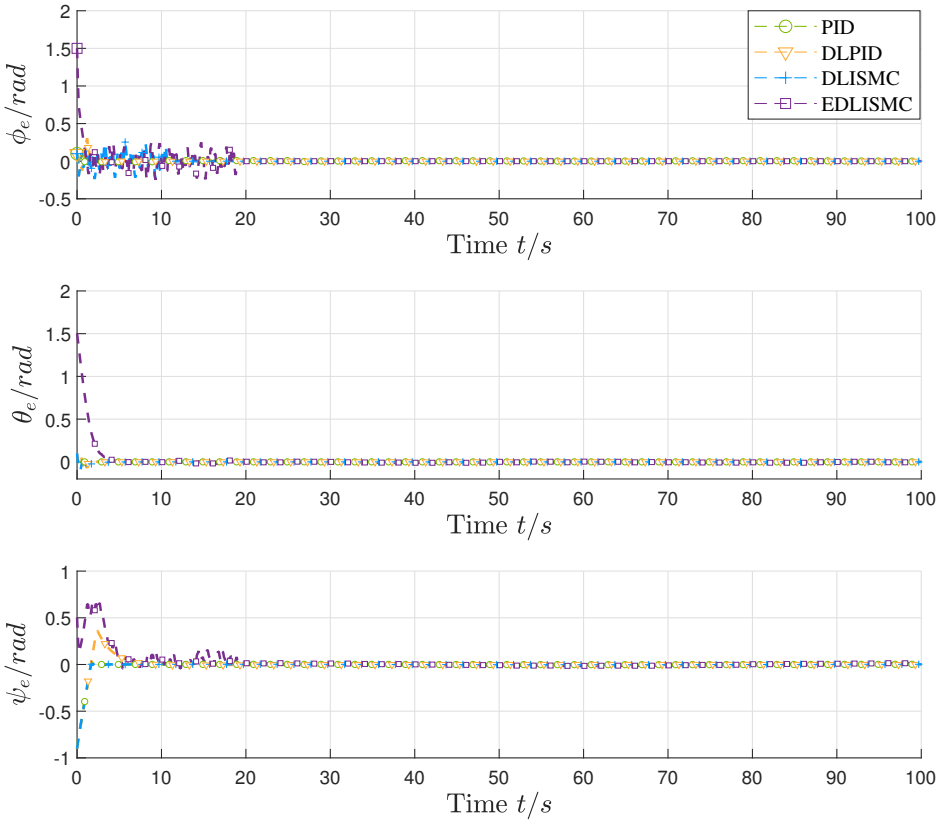


Figure 7. Angular tracking error of different control methods in Scenario 1.

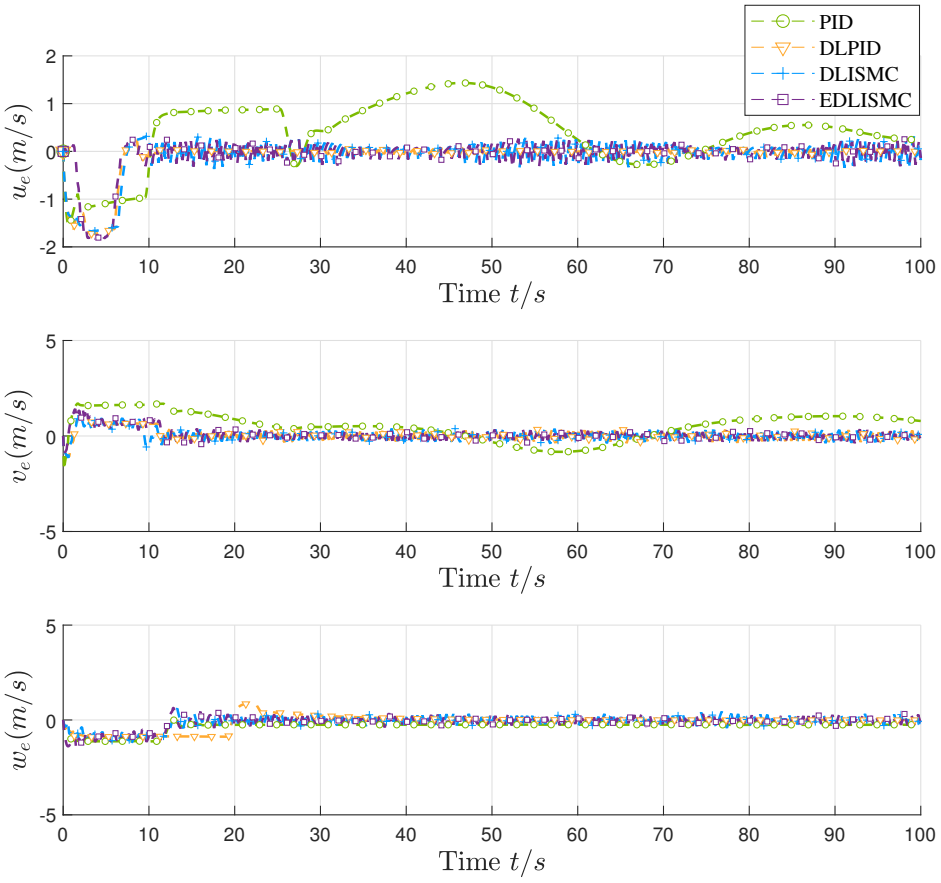


Figure 8. Linear velocity tracking error of different control methods in Scenario 1.

Figure 11 shows the trigger intervals of different thrusts τ_u, τ_v, τ_w, τ_p, τ_q, and τ_r in Scenario 1, where the horizontal coordinate of each vertical line is the specific time of a trigger, and the vertical coordinate is the time difference between this trigger and the previous trigger. It can be found from Table 3 that the trigger interval of EDLISMC is much larger than the fixed time trigger interval of 0.1 s. Hence, without the need for the frequent update of control signals, EDLISMC can maintain stability and good control performance. Compared with DLISMC based on fixed-time triggering, EDLISMC reduces the output frequency of control signals effectively and the occupation of system communication and computing resources through the event triggering mechanism, which improves the resource utilization efficiency of the UUV.

Table 3. Statistical result of different triggering mechanisms in Scenario 1.

Triggering Item	Triggering Count	Event Triggering Count/Time Triggering Count
Time triggering mechanism	1000	/
τ_u	296	29.6%
τ_v	351	35.1%
τ_w	370	37.0%
τ_p	204	20.4%
τ_q	362	36.2%
τ_r	807	80.7%

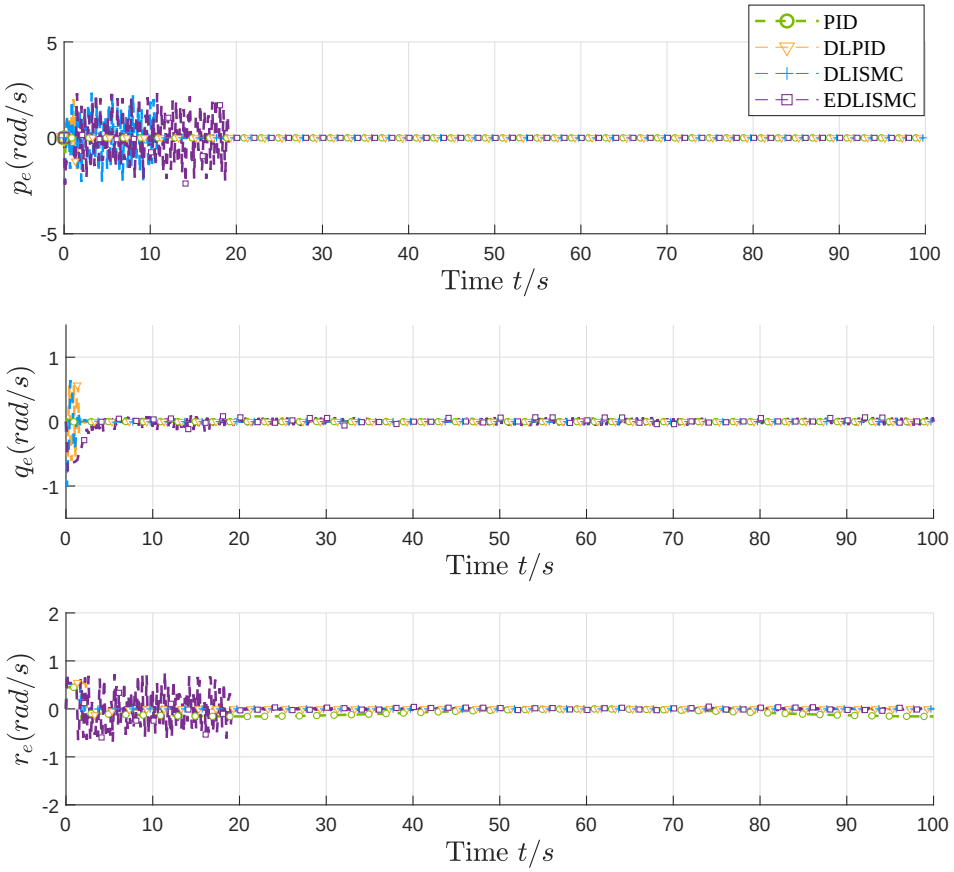


Figure 9. Angular velocity tracking error of different control methods in Scenario 1.

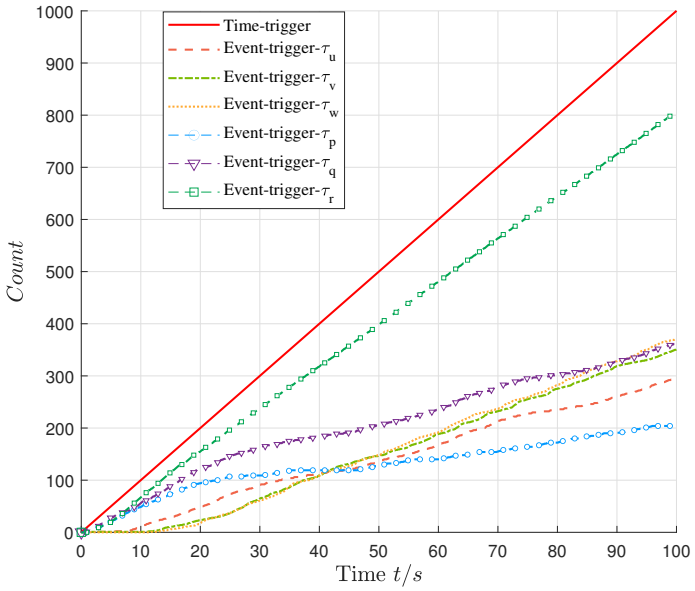


Figure 10. Triggering frequencies of different thrusts in Scenario 1.

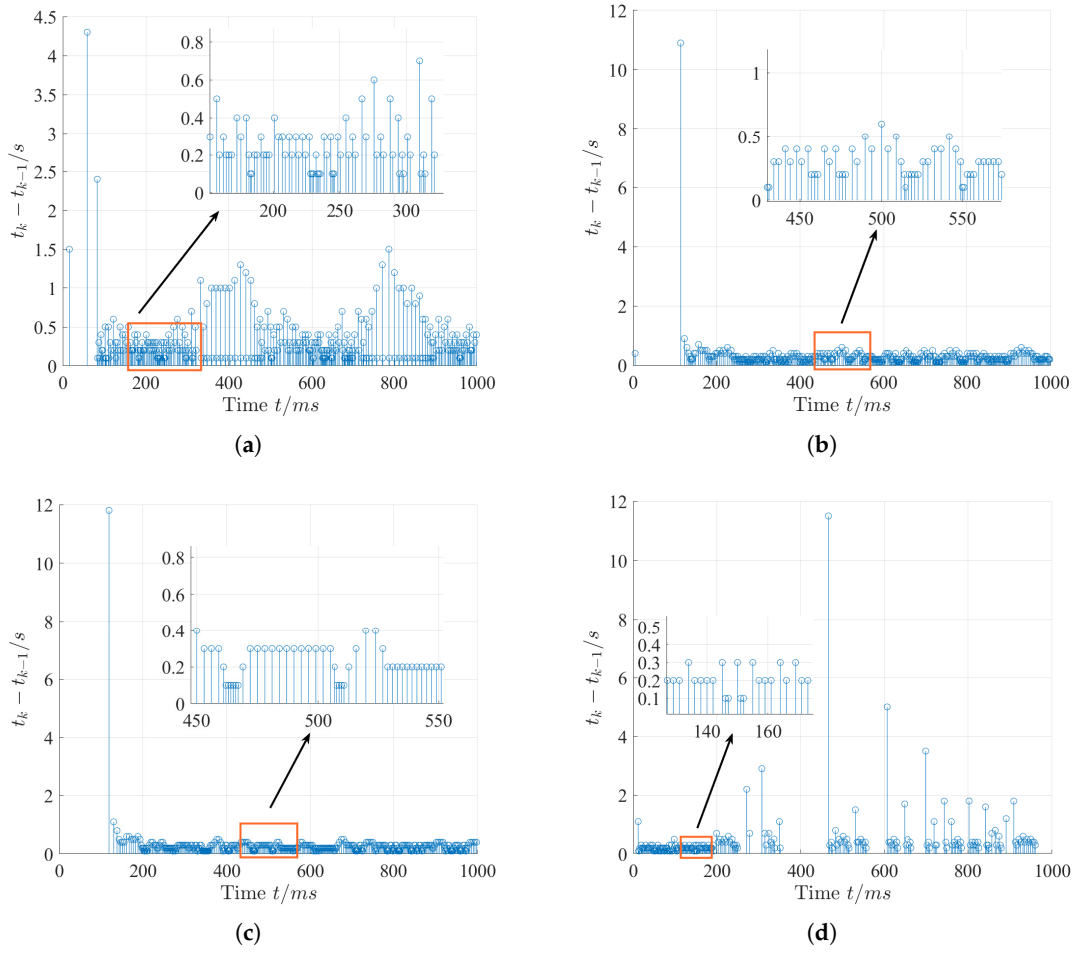
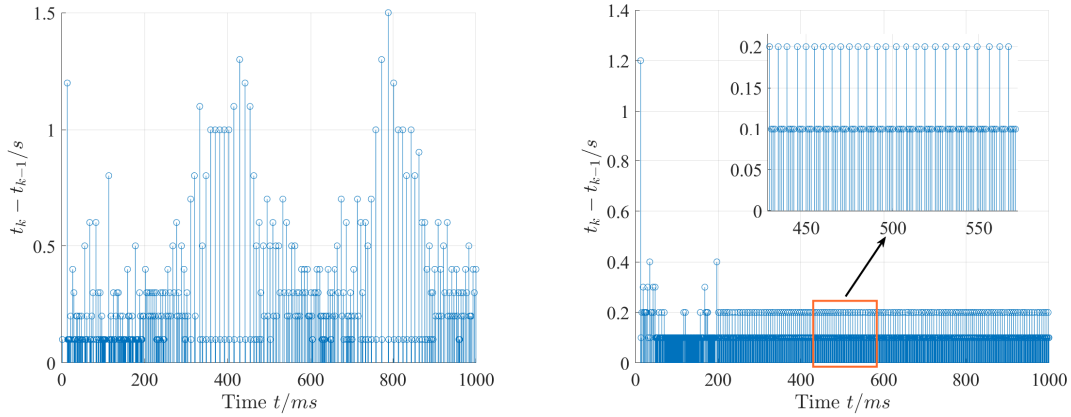


Figure 11. *Cont.*



(**e**) (**f**)

Figure 11. Triggering interval of different thrusts in Scenario 1. (**a**) The triggering interval of τ_u in Scenario 1. (**b**) The triggering interval of τ_v in Scenario 1. (**c**) The triggering interval of τ_w in Scenario 1. (**d**) The triggering interval of τ_p in Scenario 1. (**e**) The triggering interval of τ_q in Scenario 1. (**f**) The triggering interval of τ_r in Scenario 1.

5.2.2. Results of Scenario 2

In Scenario 2, the UUV verifies the tracking performance of the EDLISMC controller through three-dimensional spatial spiral trajectory tracking, where the experimental duration is 100 s. In the geodetic coordinate framework, the ideal planar cosine trajectory can be described by the following equation:

$$\begin{cases} x_d(t) = 0.25 \times t \\ z_d(t) = 0 \\ \theta_d(t) = 0 \\ \phi_d(t) = 0 \\ y_d(t) = 10 \times \sin(0.025\pi t) \\ \psi_d(t) = \cos(0.025\pi t) \end{cases} \tag{57}$$

Figure 12 shows a three-dimensional spatial graph of UUV trajectory tracking under different control methods in Scenario 2. In Figure 12, the red star is used to represent the starting position of the UUV, and the blue star is used to represent the end point of the UUV. After the experiment starts, the UUV starts to move according to different control methods, respectively. Although all four methods can track the expected trajectory eventually, EDLISMC tracks the expected trajectory earlier than other methods.

Figure 13 is the location tracking error of the UUV in Scenario 2, where the location tracking errors of all control methods converge to 0.05 m. Compared with Scenario 1, the motion trajectory in Scenario 2 is more complex and changeable, which puts forward higher requirements for control methods. In addition, compared with PID and DLPID, DLISMC and EDLISMC show more superior convergence performance, which can reduce location errors more quickly and enable the UUV to track the expected trajectory more rapidly.

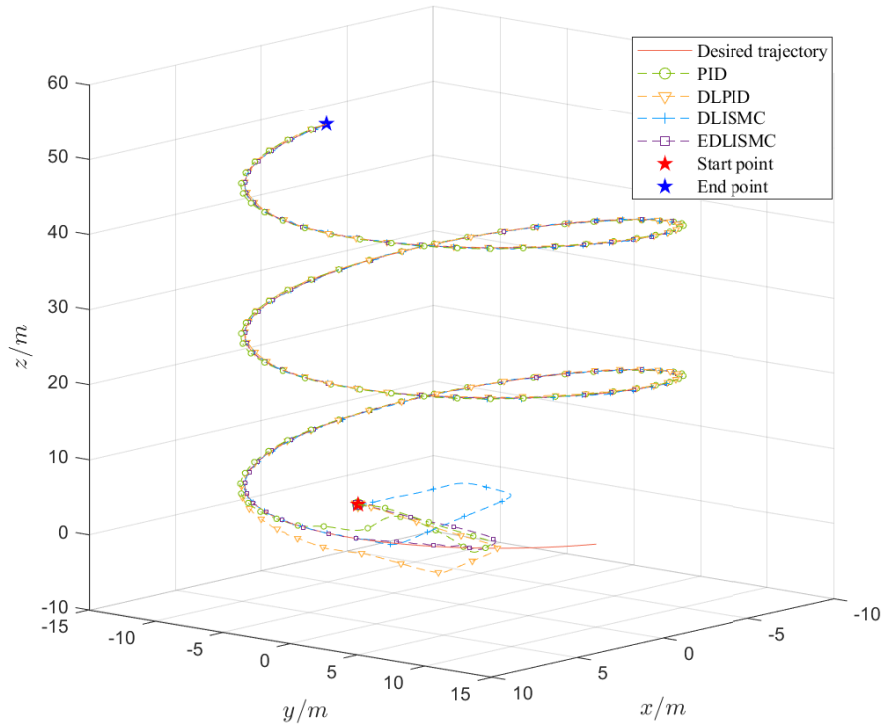


Figure 12. Trajectory tracking of different control methods in Scenario 2.

Figure 14 is the angular tracking error of the UUV in Scenario 2, where the angular tracking errors of all control methods converge to 0.01 rad. It can be seen from Figure 14 that the four methods can control the angular deviation of the UUV effectively. The error of EDLISMC is relatively large in the initial stage. The reason for this phenomenon is that the rapid response of the system to the control signal leads to instantaneous overshoot. As time increases, the error of EDLISMC decreases rapidly and tends to be stable finally, which indicates that EDLISMC has strong dynamic adjustment ability and can correct angular errors in a short time.

In Scenario 2, Figures 15 and 16 are the tracking errors of UUV for linear velocity and angular velocity, respectively, where the linear velocity tracking errors of all control methods converge to 0.2 m/s, and the angular velocity tracking errors of all control methods converge to 0.05 rad/s. In Figure 15, all control methods achieve the convergence of linear velocity tracking error. PID has significant initial fluctuations and slower convergence rates in all three directions, which proves that PID has limited adaptability for nonlinearities and disturbances. Although DLPID outperforms PID in terms of error convergence speed and stability, it still shows a certain degree of steady-state fluctuations. DLISMC converges the errors to near zero in all directions. Compared to other methods, EDLISMC has the fastest error convergence speed, the smallest steady-state error, and the least jitter.

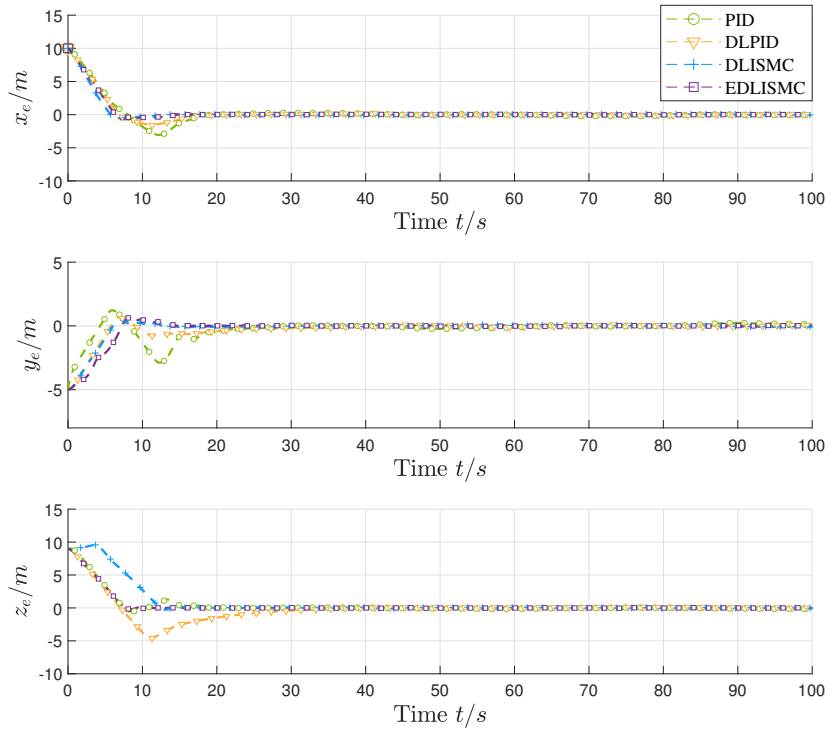


Figure 13. Location tracking error of different control methods in Scenario 2.

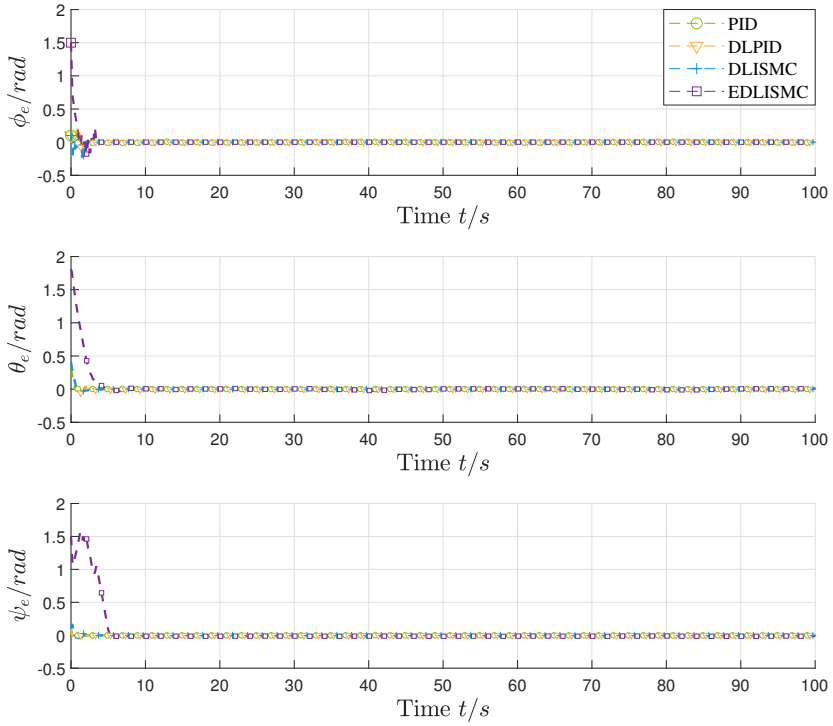


Figure 14. Angular tracking error of different control methods in Scenario 2.

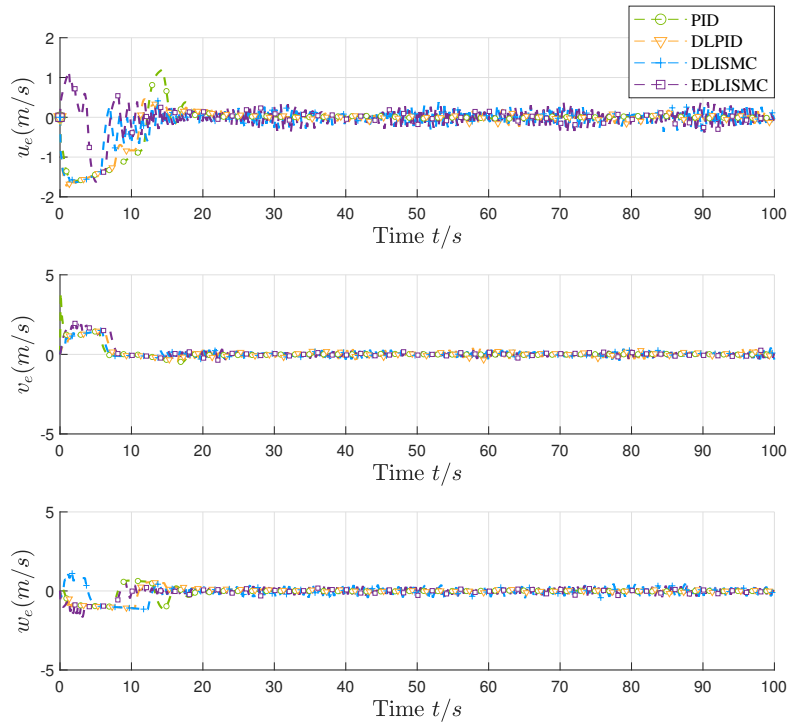


Figure 15. Linear velocity tracking error of different control methods in Scenario 2.

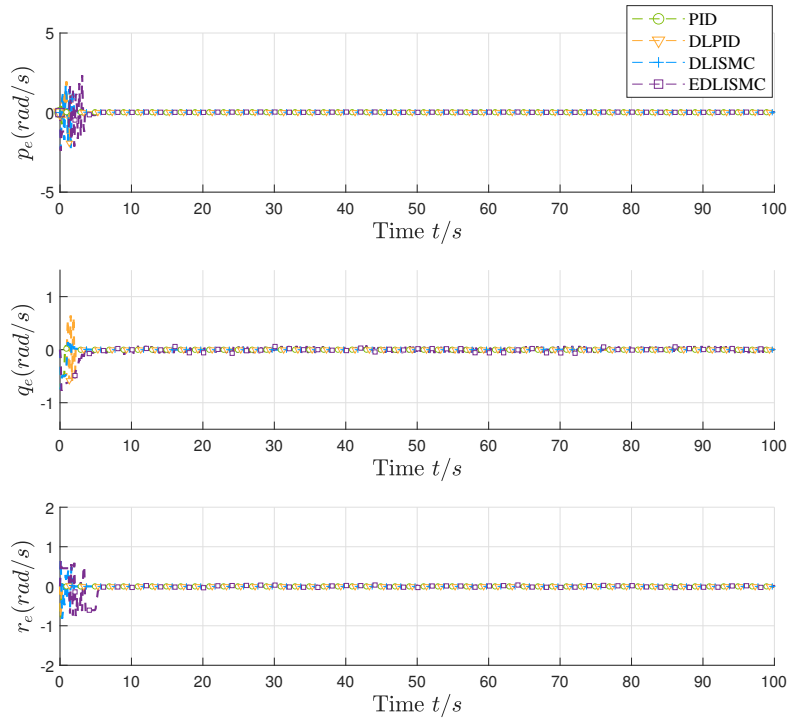


Figure 16. Angular velocity tracking error of different control methods in Scenario 2.

As shown in Figure 17, there is a significant difference in the number of trigger times between the time triggering mechanism and event triggering mechanism in Scenario 2. It can be seen from Table 4 that compared with the time triggering mechanism, the event triggering mechanism has more advantages in control signals. The event triggering mechanism only triggers control signals when the system state changes significantly or meets

preset conditions, which can avoid a large number of redundant control outputs. The time triggering mechanism sends control signals at fixed time intervals, which leads to a large number of unnecessary control signal outputs. Hence, considering the high requirements for communication costs, computing resources, and energy efficiency, the event triggering mechanism has more obvious advantages.

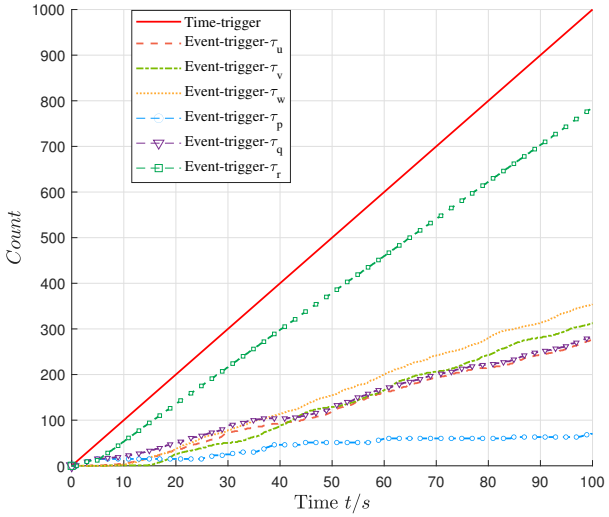


Figure 17. Triggering frequencies of different thrusts in Scenario 2.

Table 4. Statistical result of different triggering mechanisms in Scenario 2.

Triggering Item	Triggering Count	Event Triggering Count/Time Triggering Count
Time triggering mechanism	1000	/
τ_u	276	27.6%
τ_v	313	31.3%
τ_w	354	35.4%
τ_p	70	7%
τ_q	282	28.2%
τ_r	785	78.5%

Figure 18 shows the triggering interval of τ_u, τ_v, τ_w, τ_p, τ_q, and τ_r in Scenario 2, respectively. Compared to the time triggering mechanism, the event triggering mechanism has a longer triggering interval. Among them, the maximum triggering interval of τ_p is 24 s.

The simulation results from Scenario 1 and Scenario 2 verify that the proposed EDLISMC achieves stability and precision in the trajectory tracking of the UUV and demonstrates significant advantages in the output of control signals. Compared to the traditional time triggering mechanism, EDLISMC outputs control signals at necessary moments through an event triggering mechanism, which reduces the output frequency of the control signal and alleviates the communication and computational burden on UUV. Hence, EDLISMC improves the efficiency of resource utilization and extends the operational duration of UUV. When the control signal output frequency is reduced, EDLISMC maintains the trajectory tracking performance of the UUV, which demonstrates that EDLISMC can improve system efficiency and meet the stability and accuracy requirements of the UUV for trajectory tracking.

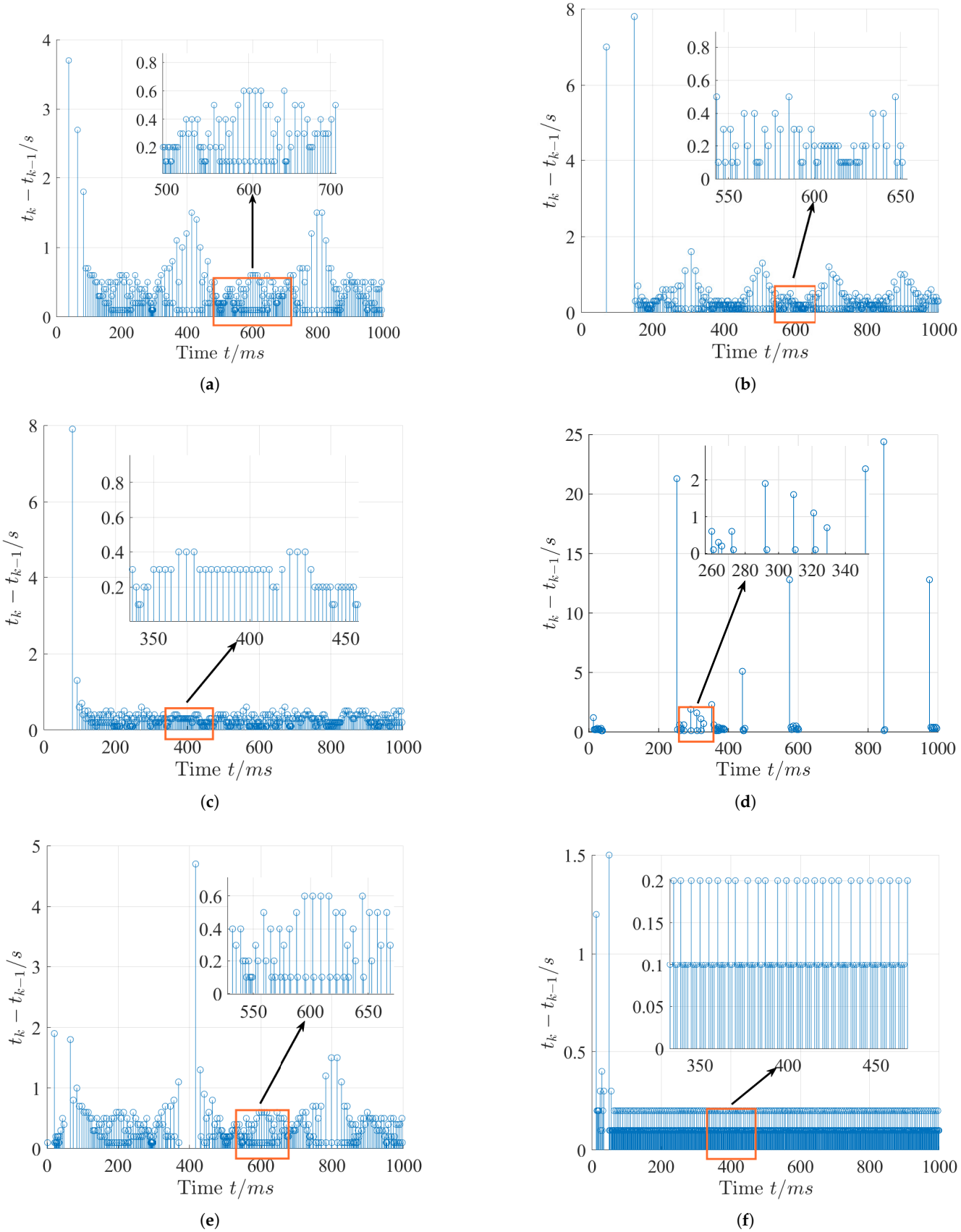


Figure 18. Triggering interval of different thrusts in Scenario 2. (**a**) The triggering interval of τ_u in Scenario 2. (**b**) The triggering interval of τ_v in Scenario 2. (**c**) The triggering interval of τ_w in Scenario 2. (**d**) The triggering interval of τ_p in Scenario 2. (**e**) The triggering interval of τ_q in Scenario 2. (**f**) The triggering interval of τ_r in Scenario 2.

In this paper, EDLISMC, DLISMC, PID, and DLPID belong to modern control, where their time complexity and space complexity is $O(n)$. Since the UUV uses embedded systems typically, the above methods do not impose a significant burden on the operational performance of the UUV. EDLISMC reduces redundant control signals, resulting in its superior performance.

6. Conclusions

This paper analyzed the 6-DOF UUV mathematical model under reaction torque and proposed EDLISMC for the trajectory tracking control of the UUV. In the dual-loop controller framework of this method, the output of the location loop controller was used as the reference speed input of the speed loop controller. Among them, the location loop controller and the speed loop controller achieved error stability through the integral sliding mode surface. Then, this method designed an event triggering function for the event triggering mechanism to reduce the triggering frequency of control signals. In terms of theoretical proof, the positive lower bound method was used to prove that the event triggering mechanism does not have Zeno behavior. In addition, this paper conducted a stability analysis of the designed controller through the Lyapunov theorem, which can prove the stability of EDLISMC. Finally, this paper performed the simulation in two typical scenarios to validate the effectiveness of EDLISMC.

Author Contributions: Writing—original draft, Y.J. and W.C.; investigation, H.C.; methodology, W.C.; resources, M.Z.; validation, Y.J.; writing—review and editing, M.Z. All authors read and agree to publish the version of this manuscript.

Funding: This research has been partially funded by Key Research and Development Program of Zhejiang Province (2023C01028), National Natural Science Foundation of China (No.62271179).

Data Availability Statement: The data or code of the research results can be obtained from the corresponding author upon reasonable request.

Conflicts of Interest: The authors declare no conflicts of interest.

References

1. Cai, W.; Chen, H.; Zhang, M. A cooperative hunting algorithm based on performance level classification for multi-autonomous underwater vehicle performance heterogeneity. *J. Braz. Soc. Mech. Sci. Eng.* **2025**, *47*, 1–16. [CrossRef]
2. Wang, H.; Han, G.; Tang, D.; Xiong, W. Multi-AUV Collaboration-Assisted Location Privacy Protection Scheme in Unknown Marine Environments. *IEEE Internet Things J.* **2024**, *11*, 27398–27408. [CrossRef]
3. Fayaz, S.; Parah, S.; Qureshi, J.; Lloret, J.; Del, J.; Muhammad, K. Intelligent underwater object detection and image restoration for autonomous underwater vehicles. *IEEE Trans. Veh. Technol.* **2023**, *73*, 1726–1735. [CrossRef]
4. Zhu, X.; Khan, A.A.S.; Li, X. Global lumped mass formulation for underwater cable dynamics. *Nonlinear Dyn.* **2025**, *113*, 989–1006. [CrossRef]
5. Er, M.J.; Gong, H.; Liu, Y.; Liu, T. Intelligent trajectory tracking and formation control of underactuated autonomous underwater vehicles: A critical review. *IEEE Trans. Syst. Man Cybern. Syst.* **2023**, *54*, 543–555. [CrossRef]
6. Ma, D.; Chen, X.; Ma, W.; Zheng, H.; Qu, F. Neural Network Model-Based Reinforcement Learning Control for AUV 3-D Path Following. *IEEE Trans. Intell. Veh.* **2024**, *9*, 893–904. [CrossRef]
7. Cui, J.; Hou, M.; Peng, Z.; Wang, Y.; Cui, J.H. Hamiltonian based AUV navigation using adaptive finite-time trajectory tracking control. *Ocean Eng.* **2025**, *320*, 1–17. [CrossRef]
8. Li, X.; Liu, Y. A new fuzzy SMC control approach to path tracking of autonomous underwater vehicles with mismatched disturbances. In Proceedings of the OCEANS 2022, Chennai, India, 21–24 February 2022; pp. 1–5.
9. Zhang, W.; Wang, Q.; Du, X.; Zheng, Y. Real-time NMPC for three-dimensional trajectory tracking control of AUV with disturbances. *Ocean Eng.* **2025**, *319*, 1–13. [CrossRef]
10. Wan, L.; Zhang, Y.; Sun, Y.; Li, Y.; He, B. ADRC Path-Following Control of Underactuated AUVs. *J. Shanghai Jiao Tong Univ.* **2014**, *48*, 1727–1731.
11. Ye, H.; Wang, L.; Zhi, P.; Zhu, D. Adaptive three-dimensional path tracking control for AUV based on disturbance observer. *J. Jiangsu Univ. Sci. Technol. (Nat. Sci. Ed.)* **2019**, *33*, 52–59.

12. Wang, Y.; Hou, Y.; Lai, Z.; Cao, L.; Hong, W.; Wu, D. An expert-demonstrated soft actor–critic based adaptive trajectory tracking control of Autonomous Underwater Vehicle with Long Short-Term Memory. *Ocean Eng.* **2025**, *321*, 1–11. [CrossRef]
13. Li, G.; Li, J.; Zhong, R.; Xie, H.; Dan, Y.; Hou, C. An AUV Control Method Based on Modified Super-Twisting Sliding Mode and Disturbance Observer. *Digit. Ocean. Underw. Warf.* **2023**, *6*, 300–307.
14. Li, J.; Xia, Y.; Xu, G.; Guo, Z.; Han, H.; Wu, Z.; Xu, K. Enhanced three-dimensional trajectory tracking control for AUVs in variable operating conditions using FMPC-FTTSMC. *Ocean Eng.* **2024**, *310*, 1–19. [CrossRef]
15. Xu, X.; He, B.; Dai, N.; Wang, T.; Shen, Y. Tracking control study of AUV large curvature path based on artificial physics method. *Ocean Eng.* **2024**, *303*, 1–15. [CrossRef]
16. Li, B.; Gao, X.; Huang, H.; Yang, H. Improved adaptive twisting sliding mode control for trajectory tracking of an AUV subject to uncertainties. *Ocean Eng.* **2024**, *297*, 1–12. [CrossRef]
17. Chen, P.; Yu, L.; Guo, K.; Qiao, L. Fast and Accurate Trajectory Tracking Control for Underactuated AUVs With Mismatched Disturbances: Theory and Experiment. *IEEE Trans. Ind. Electron.* **2025**, *99*, 1–10. [CrossRef]
18. Fenco Bravo, L.P.; Pérez Zuñiga, C.G. Nonlinear trajectory tracking with a 6DOF AUV using an MRAFC controller. *IEEE Lat. Am. Trans.* **2025**, *23*, 160–171. [CrossRef]
19. Ebrahimpour, M.; Lungu, M. Finite-Time Path-Following Control of Underactuated AUVs with Actuator Limits Using Disturbance Observer-Based Backstepping Control. *Drones* **2025**, *9*, 70. [CrossRef]
20. Xu, F.; Zhang, L.; Zhong, J. Three-dimensional path tracking of over-actuated AUVs based on mpc and variable universe s-plane algorithms. *J. Mar. Sci. Eng.* **2024**, *12*, 418. [CrossRef]
21. Yu, G.; He, F.; Liu, H. Fuzzy neural network adaptive AUV control based on FTHGO. *Sh. Offshore Struct.* **2025**, *20*, 13–25. [CrossRef]
22. Miao, J.; Wang, S.; Zhao, Z.; Li, Y.; Tomovic, M.M. Spatial curvilinear path following control of underactuated AUV with multiple uncertainties. *ISA Trans.* **2017**, *67*, 107–130. [CrossRef] [PubMed]
23. Al Makdah, A.A.R.; Daher, N.; Asmar, D.; Shammas, E. Three-dimensional trajectory tracking of a hybrid autonomous underwater vehicle in the presence of underwater current. *Ocean Eng.* **2019**, *185*, 115–132. [CrossRef]
24. Pan, Y.; Yang, C.; Pan, L.; Yu, H. Integral sliding mode control: Performance, modification, and improvement. *IEEE Trans. Ind. Inform.* **2017**, *14*, 3087–3096. [CrossRef]
25. Abidi, K.; Xu, J.X.; Xinghuo, Y. On the discrete-time integral sliding-mode control. *IEEE Trans. Autom. Control* **2007**, *52*, 709–715. [CrossRef]
26. Song, L.; Tong, S. Finite-time resilient integral sliding-mode control for fuzzy impulsive stochastic system under denial-of-service attacks. *IEEE Trans. Fuzzy Syst.* **2024**, *32*, 2930–2939. [CrossRef]
27. Binh, T.N.; Huu Sau, N.; Thi Thanh Huyen, N.; Thuan, M.V. Guaranteed cost control of delayed conformable fractional-order systems with nonlinear perturbations using an event-triggered mechanism approach. *Int. J. Syst. Sci.* **2025**, *74*, 1–18. [CrossRef]
28. Liu, G.P. Tracking control of multi-agent systems using a networked predictive PID tracking scheme. *IEEE/CAA J. Autom. Sin.* **2023**, *10*, 216–225. [CrossRef]
29. Ji, Y.; Zhang, J.; Zhang, J.; He, C.; Hou, X.; Han, J. Constraint performance slip ratio control for vehicles with distributed electrohydraulic brake-by-wire system. *Proc. Inst. Mech. Eng. Part D J. Automob. Eng.* **2024**, *238*, 1861–1879. [CrossRef]
30. Guerrero, J.; Torres, J.; Creuze, V.; Chemori, A. Adaptive disturbance observer for trajectory tracking control of underwater vehicles. *Ocean Eng.* **2020**, *200*, 107080. [CrossRef]
31. Herman, P. Numerical Test of Several Controllers for Underactuated Underwater Vehicles. *Appl. Sci.* **2020**, *10*, 8292. [CrossRef]

Disclaimer/Publisher's Note: The statements, opinions and data contained in all publications are solely those of the individual author(s) and contributor(s) and not of MDPI and/or the editor(s). MDPI and/or the editor(s) disclaim responsibility for any injury to people or property resulting from any ideas, methods, instructions or products referred to in the content.